A SEARCH FOR YOUNG STELLAR OBJECTS IN MBM 12

by

ADAM SCHNEIDER

(Under the Direction of Loris Magnani)

ABSTRACT

This work addresses the current state of star formation within the high-latitude molecular cloud MBM 12. We use new Spitzer Space Telescope observations at 3.6, 4.5, 5.8, 8.0, 24, and 70 μm to find new candidate young stellar objects (YSOs). The candidates are identified by means of visual inspection of the image data, color – magnitude and color – color diagrams, and the shape of their spectral energy distributions. Comparisons to the known YSOs residing in this region are used to examine the cloud's star formation history. With these techniques, we create a list of possible YSO candidates for further investigation.

INDEX WORDS: Molecular clouds, MBM 12, Infrared observations, Star formation

A SEARCH FOR YOUNG STELLAR OBJECTS IN MBM 12

by

ADAM SCHNEIDER

B.S., The University of Georgia, 2006

A Thesis Submitted to the Graduate Faculty of The University of Georgia in Partial Fulfillment
of the Requirements for the Degree

MASTER OF SCIENCE

ATHENS, GEORGIA

2008

A SEARCH FOR YOUNG STELLAR OBJECTS IN MBM 12

by

ADAM SCHNEIDER

Major Professor: Loris Magnani

Committee: Jean-Pierre Caillault
Robin Shelton

Electronic Version Approved:

Maureen Grasso
Dean of the Graduate School
The University of Georgia
August 2008

ACKNOWLEDGEMENTS

I would like to extend thanks first and foremost to Loris Magnani for his extensive help in the construction and writing of this thesis. I would also like to thank my committee members, Dr. Caillault and Dr. Shelton for their valuable input. Many thanks also go to Bill Reach at the Spitzer Science Center (SSC) for sharing with me his Spitzer analysis expertise. Thank you also to Peregrine McGehee for the Sloan Digital Sky Survey data, and Marc Pound for the CO data. Finally, I must thank my family and wonderful girlfriend for all of their support, I love you all.

We thank those who have been involved in the Spitzer mission. This work was based on observations made with the Spitzer Space Telescope which is operated by the Jet Propulsion Laboratory , California Institute of Technology, under NASA contract 1407. Support for this work was provided by NASA through an award issued by JPL/Caltech.

Funding for the SDSS and SDSS-II has been provided by the Alfred P. Sloan Foundation, the Participating Institutions, the National Science Foundation, the U.S. Department of Energy, the National Aeronautics and Space Administration, the Japanese Monbukagakusho, the Max Planck Society, and the Higher Education Funding Council for England. The SDSS Web Site is http://www.sdss.org/.

The SDSS is managed by the Astrophysical Research Consortium for the Participating Institutions. The Participating Institutions are the American Museum of Natural History, Astrophysical Institute Potsdam, University of Basel, University of Cambridge, Case Western Reserve University, University of Chicago, Drexel University, Fermilab, the Institute for Advanced Study, the Japan Participation Group, Johns Hopkins University, the Joint Institute for Nuclear Astrophysics, the Kavli Institute for Particle Astrophysics and Cosmology, the Korean Scientist Group, the Chinese Academy of Sciences (LAMOST), Los Alamos National Laboratory, the Max-Planck-Institute for Astronomy (MPIA), the Max-Planck-Institute for Astrophysics (MPA), New Mexico State University, Ohio State University, University of Pittsburgh, University of Portsmouth, Princeton University, the United States Naval Observatory, and the University of Washington.

This publication makes use of data products from the Two Micron All Sky Survey, which is a joint project of the University of Massachusetts and the Infrared Processing and Analysis Center/California Institute of Technology, funded by the National Aeronautics and Space Administration and the National Science Foundation.

This research has made use of the SIMBAD database, operated at CDS, Strasbourg, France.

.

TABLE OF CONTENTS

LIST OF TABLES

Page

LIST OF FIGURES

Page

Chapter 1: Introduction

1.1 Stars and Gas in the Galaxy

Galaxies dominate the luminous landscape of our Universe. To understand how these massive systems function, we must attempt to grasp the processes occurring within them. The most important of these is star formation. As galaxies are building blocks of the Universe, stars are the building block of galaxies. Approximately eighty to ninety percent of the total mass of all ordinary baryonic matter in a typical spiral galaxy is made up of stars. The remainder of the baryonic matter is almost entirely in the form of gas and dust. This gas is found in both atomic and molecular forms. Comprehending the molecular component of this gas is crucial for the issue of star formation because virtually all stars form from molecular "clouds"[1]. Under certain conditions, small, dense clumps within molecular clouds collapse and initiate the processes that will eventually form young stellar objects (YSOs). The manner in which a clump of molecular gas evolves into a protostar is still not entirely understood, though great strides have been made in the last two decades (Smith 2004).

Not surprisingly, molecular gas in the Galaxy is primarily made up of H_2, hydrogen being the most abundant element in the universe. Unfortunately, interstellar H_2 is very difficult to observe directly from the Earth's surface. The relevant rotational, vibrational, and electronic transitions lie in the infrared or ultraviolet portion of the electromagnetic spectrum and are

[1] Concentrations of molecular gas in a galaxy are whimsically referred to as clouds because of their ragged shapes.

strongly absorbed by the Earth's atmosphere. Because of this, other molecules, referred to as surrogate tracers, must be used to identify the molecular regions of our Galaxy. The most important of these and the second most common molecule in the interstellar medium is carbon monoxide (CO). The lowest rotational transition of CO emits in the radio portion of the electromagnetic spectrum (2.6 mm), and is readily observed with ground based millimeter-wave radio telescopes. By means of CO observations, much of the molecular gas in the Milky Way has been mapped (Dame, Hartmann, & Thaddeus 2001). It has been established by large-scale CO surveys that giant molecular clouds (GMCs) comprise the majority of the molecular mass in the Galaxy. These are massive, gravitationally bound objects with typical masses of 10^4 -10^6 $M_\odot$[2]. GMCs are generally located in the disk of our Galaxy and form large and small stars readily. Many smaller molecular clouds ($\leq 10^3$ $M_\odot$) have also been found, and also tend to exist throughout the galactic plane. Smaller clouds are categorized into three types based on visual extinctions (A_v) along the line of sight through the cloud: diffuse, translucent, and dark (van Dishoeck & Black 1988). Diffuse clouds are defined as those that have $A_v < 1$ magnitude. Likewise, dark clouds are defined to have $A_v > 5$ magnitudes. Translucent clouds are those that have intermediate extinctions ($1 \leq A_v \leq 5$ mag). These distinctions also help to discriminate between the different astrochemical processes occurring within the clouds. Diffuse clouds are permeated by interstellar UV radiation, and their chemistry is thus governed mostly by photochemical processes. Dark clouds have much dust, which absorbs UV light, forcing the chemistry to proceed primarily by collisional processes. In translucent clouds, both collisional and photochemical processes are critical to their chemical evolution.

[2] $M_\odot$ signifies one solar mass ($\approx 1.989 \times 10^{30}$ kg)

While GMCs give rise to high and low mass stars, small molecular clouds form only low mass stars ($M \leq 8\ M_{\odot}$). However, not all types of small molecular clouds are suitable for star formation. Dark clouds certainly are, diffuse clouds certainly are not, and the star formation status of translucent clouds is somewhat uncertain (Hearty 1997). While it is clear that translucent clouds with visual extinctions everywhere less than 2 magnitudes do not form stars (Hearty et al. 1999), clouds near the translucent/dark extinction border are known to give rise to low mass star formation (e.g., MBM 12, MBM 20)[3]. This capability seems independent of dynamical states: MBM 12 contains dense clumps that are not gravitationally bound to the cloud itself (Pound, Bania, & Wilson 1990), while MBM 20 is a gravitationally bound entity (Liljestrom 1991).

The first step to understanding what factors trigger star formation in some of the more opaque translucent clouds is to assess the star forming history of the cloud in question. In this thesis, we use high quality data from the Spitzer infrared space telescope to compile several different types of catalogs of possible newly-formed stars within and near the translucent/dark cloud MBM 12. These catalogs will provide the springboard for future optical studies of the star-forming potential and history of this object. MBM 12 is also known as a Lynds Dark Nebula comprising four objects in Lynds (1962) dark cloud catalog (L1453, L1454, L1457, L1458). It is also one of the original high-latitude molecular clouds identified by Magnani, Blitz, & Mundy (1985). We will now discuss the relationship between high-latitude molecular clouds and translucent clouds.

---

[3] MBM 12 currently has 11 T Tauri stars associated with it (Luhman 2001). MBM 20 has at least 4 pre-main sequence stars within its confines (Sandell et al. 1987).

1.2 High Latitude Clouds

High latitude molecular clouds are those with a galactic latitude (*b*) greater than 25° or less than -25° and were identified as a class of objects by Magnani, Blitz, & Mundy (1985). Like these authors, we have chosen $|b| = 25°$ as the boundary of the high-latitude regime in order to exclude those clouds that are connected with large-scale molecular structures extending to higher latitudes (e.g. the Ophiuchus Cloud Complex and the Taurus-Auriga dark clouds). In this way, high-latitude clouds comprise a distinct cloud population. There is also likely a dynamic distinction between high-latitude clouds and the small clouds residing at $|b| \leq 25° - 30°$ (Magnani, Hartmann, & Speck 1996). Most of the high-latitude clouds are thought to form along the edges of shells compressed by expansion waves in the interstellar medium (Gir, Blitz, & Magnani 1994). Given the thinness of the molecular disk of the Galaxy (Gaussian thickness ~ 87 pc; Dame, Hartmann, & Thaddeus 2001), the high galactic latitude of these clouds ensures that they are relatively local: no more than a few hundred parsecs from the Sun (Magnani, Hartmann, & Speck 1996). Thus, they are definitely a disk population of objects. However, it is their proximity to the Sun that makes their study particularly worthwhile. Observations of high-latitude molecular clouds provide the highest spatial resolution possible for any type of molecular cloud.

The majority of high latitude clouds are of the translucent variety, making them difficult to detect using photographic surveys. Some of the first high-latitude clouds were noticed when Lynds (1962) identified hundreds of "dark nebulae" based on visual recognition of regions of obscuration by dust, producing a marked decrease in the stellar density compared to non-obscured regions. Almost all of these dark nebulae were determined to also contain substantial molecular gas after Dickman (1975) surveyed a large number of them in CO.

Of the more than 1800 dark clouds cataloged by Lynds, only a dozen were detected at high galactic latitudes (|*b*| > 25°). Magnani, Blitz, & Mundy (1985) increased the number of molecular clouds at |*b*| > 20° (which was the criterion for their search) by a factor of five during the course of their high-latitude CO survey. Candidates for this survey were found by searching for evidence of optical obscuration on Palomar Observatory Sky Survey (POSS) prints, just as Lynds had done, but the selected candidate regions had significantly lower extinctions. Subsequent systematic surveys for CO(1-0) emission of the northern (Hartmann et al. 1998) and southern (Magnani et al. 2000) galactic hemispheres have been carried out to add to the total number of clouds found, and more than 100 are currently known to exist.

More than 90% of all the known high-latitude clouds are translucent clouds. As such, the high-latitude clouds comprise the largest inventory of translucent molecular clouds currently known. As previously mentioned, the star forming capability of translucent clouds is uncertain. Only a half-dozen or so objects have been adequately studied (see Hearty 1997 and McGehee 2008 for a review). Of these clouds, MBM 12 has been the most extensively studied, leading to the identification of a group of T Tauri stars, or a T-association, of eleven or twelve objects[4]. Among the high-latitude clouds, MBM 12 and MBM 20 straddle the border between the definitions of translucent and dark molecular clouds (i.e., they have visual extinctions in their most opaque cores of at least 4-5 magnitudes). Perhaps not surprisingly, both objects have given rise to significant star formation. Having given a general introduction to high-latitude clouds, we will now discuss what is meant by "newly-formed" stars.

---

[4] Eleven T Tauri stars are in the immediate environs of MBM 12 and another object is located 2.5° degrees away and may be associated with MBM 13.

1.3 Young Stellar Objects

Currently, all stars in the Galaxy form within molecular clouds. Although the formation of stars from collapsing cores to Zero-Age Main Sequence (ZAMS) stars is rapid compared to the lifetime of the star on the main sequence (e.g., Bohm-Vitense 1992), there are several observationally distinct stages a star can go through as it evolves from a collapsing core to the ZAMS.

Young Stellar Objects (YSOs), a term coined by S. Strom in 1972 to encompass all pre-main-sequence stellar objects, embedded or visible, can be grouped into various classes (Shu, Adams, & Lizano 1987). The degree to which the object is dust-embedded from most to least corresponds to Classes 0, I, II, and III. Specifically, Class I YSOs are those that are deeply embedded in their dust cocoon. They are rarely detected optically and include Herbig-Haro objects. The spectral energy distributions (SEDs) of Class I YSOs tend to peak at far-infrared and sub-millimeter wavelengths. Because they are so deeply embedded, their SEDs show a large excess of infrared emission compared to that of a normal stellar photosphere. Class II YSOs are those that have substantial circumstellar disks and ongoing accretion. Classical T Tauri stars are included among Class II objects. The SED of a Class II object is broader than a single blackbody and tends to peak at the visible or near-infrared wavelengths. A Class III designation corresponds to a YSO with a reddened photosphere. These latter objects are, at times, difficult to distinguish from main-sequence stars. A fourth class of YSO, called Class 0, are those that have even redder SEDs than Class I's with extremely faint central objects. They are essentially protostars that are in the final stages of collapse and are deeply embedded in molecular cores. Because this stage is very rapid and the protostars are deeply embedded, these objects are very difficult to detect.

1.4 Outline of Thesis

The main issue this thesis will address is the current role of star formation in the translucent molecular cloud MBM 12. The question as to whether or not the young T Tauri type stars that are already known to exist in this cloud are the only stars that have formed in it will be addressed in detail. We will describe past observations of MBM 12 and its known YSOs and provide new insight into the cloud's current state of star formation by analysis of new Spitzer space telescope infrared data. Chapter 2 will provide a description of the high-latitude molecular cloud MBM 12 and its previously known star formation history. We will then discuss briefly the Spitzer space telescope, the method by which data were taken, and the various images that were obtained as part of this project in Chapter 3. Chapter 4 will present all plots and tables resulting from the Spitzer data, along with methods used to compile the two catalogs of potential YSOs. We will then produce spectral energy distributions for the objects in the YSO catalogs in order to identify the most promising candidate YSOs in MBM 12 in Chapter 5. In Chapter 6, a discussion of the results and implications of our catalogs along with a discussion of possible follow up work that should be considered to confirm or reject potential YSO candidates will then conclude this work.

Chapter 2: MBM 12

2.1 Introduction and Distance Considerations

MBM 12 is a high latitude cloud located, in galactic coordinates, at l = 159.35° and b = -34.32°. Figure 2-1 shows a map of the color excess[5] from the Schlegel, Finkbeiner, and Davis (1999) database centered on the cloud position. The color excess is proportional to the dust column density (if the dust properties are uniform throughout the region), which, in turn, is proportional to the gas column density for a constant gas to dust ratio. Chastain et al. (2006) have shown that the Schlegel, Finkbeiner, and Davis (1998) color excess maps are excellent tracers of translucent gas so that the map shown in Figure 2-1 is an accurate depiction of the molecular gas distribution. CO was first detected in these dark clouds by Dickman (1975). In a more detailed survey of this area, Magnani, Blitz, and Mundy (1985) included this region in their catalog of high-latitude clouds as MBM 11, 12, and 13, and a poorly sampled CO map was presented by Hobbs et al. (1986). Within its molecular environs, MBM 12 contains the dark clouds Lynds 1453, 1454, 1457, and 1458. L1457 is one of the few high latitude dark clouds with $A_v > 5$ (McGehee 2008). Pound, Bania, and Wilson made a complete CO(1-0) map of the region at 1.7' resolution in 1990 and a map based on their data is shown in Figure 2-2.

Many of the physical characteristics of MBM 12 were determined by Pound, Bania, & Wilson (1990). Although a distance of 65 pc was used for their analysis, instead of the currently

---

[5] The color excess, also known as E(B-V), is defined as $(B\text{-}V)_{actual} - (B\text{-}V)_o$, where B is the blue magnitude of an object, V is the visual magnitude, $(B\text{-}V)_{actual}$ is measured for the given line of sight, and $(B\text{-}V)_o$ is what the stellar colors would be if there was no dust along the line of sight to the star.

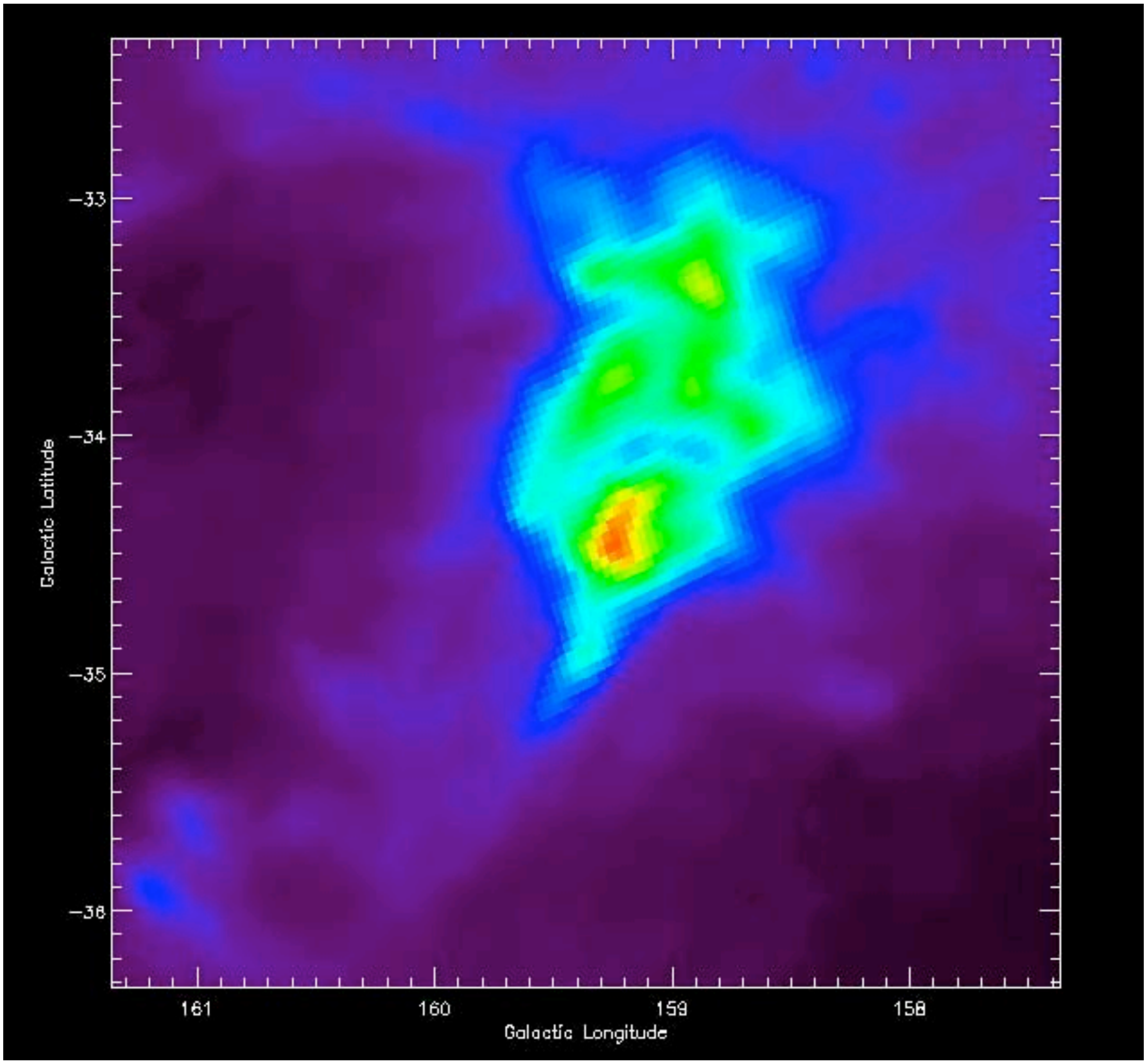

Figure 2-1. Color excess map centered on the cloud MBM 12 from Schlegel, Finkbeiner, and Davis (1998). The colors linearly depict a range of E(B-V) from 0.08 to 2.18 magnitudes. For normal dust distributions, the conversion from color excess to visual extinction, A_v, is through a multiplicative factor with value ~ 3.

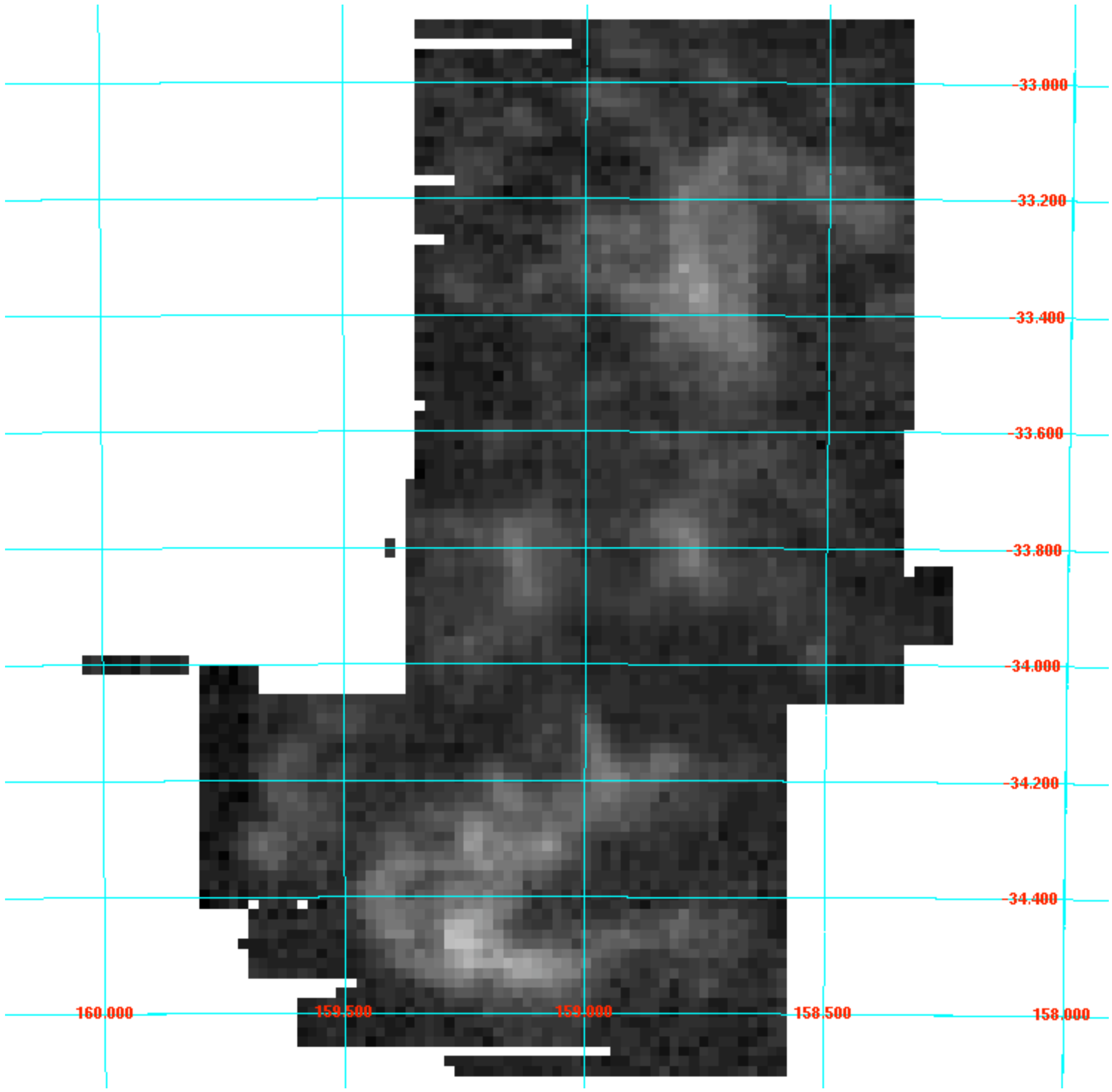

Figure 2-2. Integrated CO(1-0) map of MBM 12 in galactic coordinates. This data were kindly provided by Marc Pound. The resolution of this map is 1.7’. The lowest portion of the cloud is sometimes referred to as the “horseshoe” because of its shape.

accepted value (275 pc – see below), many of their results are still valid. Their analysis of $^{12}CO(1\text{-}0)$ and $^{13}CO(1\text{-}0)$ spectra of the cloud revealed much of its kinematic nature. Most strikingly, CO line profiles were noted to be very broad. Among high-latitude clouds, only MBM 3 and MBM 55 have similarly broad profiles. Many of the spectral profiles were shown to have multiple velocity features along the line of sight, sometimes exhibiting as many as four distinct components. These features range in Local Standard of Rest (LSR) velocities from –8 to +4 km/s. Channel maps were presented by Pound, Bania, & Wilson (1990) and reveal a very complex structure and clump distribution. Mass estimates of the cloud were calculated to be approximately 30 $M_\odot$, indicating that the cloud is not gravitationally bound by comparisons to the virial mass. Zimmermann & Ungerechts (1990) also found that the cloud, as a whole, is not gravitationally bound, but they did not rule out the possibility that some of the larger cores within it could be bound.

MBM 12 is one of very few high latitude clouds known to be a prolific star-forming region. The distance estimates to this star forming region have been revised over the years. It was once thought to be the nearest molecular cloud at a distance of $58 \pm 5 < d < 90 \pm 12$ parsecs (Hearty et al. 2000). This estimate was based on the presence and absence of Na I D absorption toward two stars with known Hipparcos parallaxes. This distance estimate led to the assertion that it was the nearest molecular cloud to the Sun, likely located within the hot ionized gas of the Local Bubble. The distance to this cloud has recently been revised by looking at photometric and/or spectroscopic studies of the stars projected onto the cloud. By looking at extinction along the line of sight, Luhman (2001) suggests the cloud is at a distance of 275 pc. There is an absorbing layer at 60-90 pc, but it is made up of atomic gas. Subsequent analysis has also given distance estimates of 360 ± 30 pc (Andersson et al. 2002) and 325 pc (Straizys et al. 2002). A distance of 275 pc will be adopted for the remainder of this thesis.

New distance estimates of 275 pc (~ 4 times the original distance estimate) increase the mass calculation by a factor of 16. Because the ratio of CO-derived mass to the virial mass scales linearly with distance, the new estimate of 275 pc for the cloud does not change the state of the cloud from being unbound. However, this larger distance likely means that some of the individual clumps within the cloud are now almost certainly gravitationally bound. This should not be surprising as the presence of gravitationally bound cores in a molecular cloud is typically associated with star forming regions.

2.2 Known YSOs Within and in the MBM 12 Region

Twelve YSOs are known to be associated with MBM 12 and their names and positions are located in Table 2-1. In Figure 2-3 we show the locations of the objects superimposed on a map of the color excess (E(B-V)) from the Schlegel, Finkbeiner, and Davis (1998) database that was already shown in Fig. 2-1. The first YSO was found from its Hα emission by the objective prism Schmidt surveys (S18, Stephenson 1986). The next three were also found from their Hα emission by the Lick grism surveys (LkHα 262, LkHα 263, and LkHα 264, Herbig & Bell 1988). A fifth young stellar object was proposed based its on X-ray emission (E 02553+2018, Fleming et al. 1989). More YSOs were not identified until 2000 when Hearty et al. used ROSAT surveys combined with optical spectroscopy to discover two more T Tauris (RX J0255.4+2005 and RXJ0258.3+1947). The last five YSOs were discovered by combining infrared and optical photometry and spectroscopy (MBM 12A 8-11, Luhman 2001). Ogura et al. (2003) have

Table 2-1

Names, Positions, and Spectral Types of Known YSOs In and Around MBM 12

#	Name	α(2000)	δ(2000)	Adopted Spectral Type[6]
1	RX J0255.4+2005	02 55 25.78	20 04 51.7	K6
2	Lkhα 262	02 56 07.99	20 03 24.3	M0
3	Lkhα 263	02 56 08.42	20 03 38.6	M3
4	Lkhα 264	02 56 37.56	20 05 37.1	K5
5	E 02553+2018	02 58 11.23	20 30 03.5	K3.5
6	RX J0258.3+1947	02 58 16.09	19 47 19.6	M4.5
7	RX J0256.3+2005	02 56 17.98	20 06 09.9	M5.75
8	MBM 12A-8	02 57 49.02	20 36 07.8	M5.5
9	MBM 12A-9	02 58 13.37	20 08 25.0	M5.75
10	MBM 12A-10	02 58 21.10	20 32 52.7	M3.25
11	MBM 12A-11	02 58 43.80	19 40 38.3	M5.5
12	S18	03 02 21.05	17 10 34.2	M3

[6] Adopted Spectral Types taken from Luhman (2001).

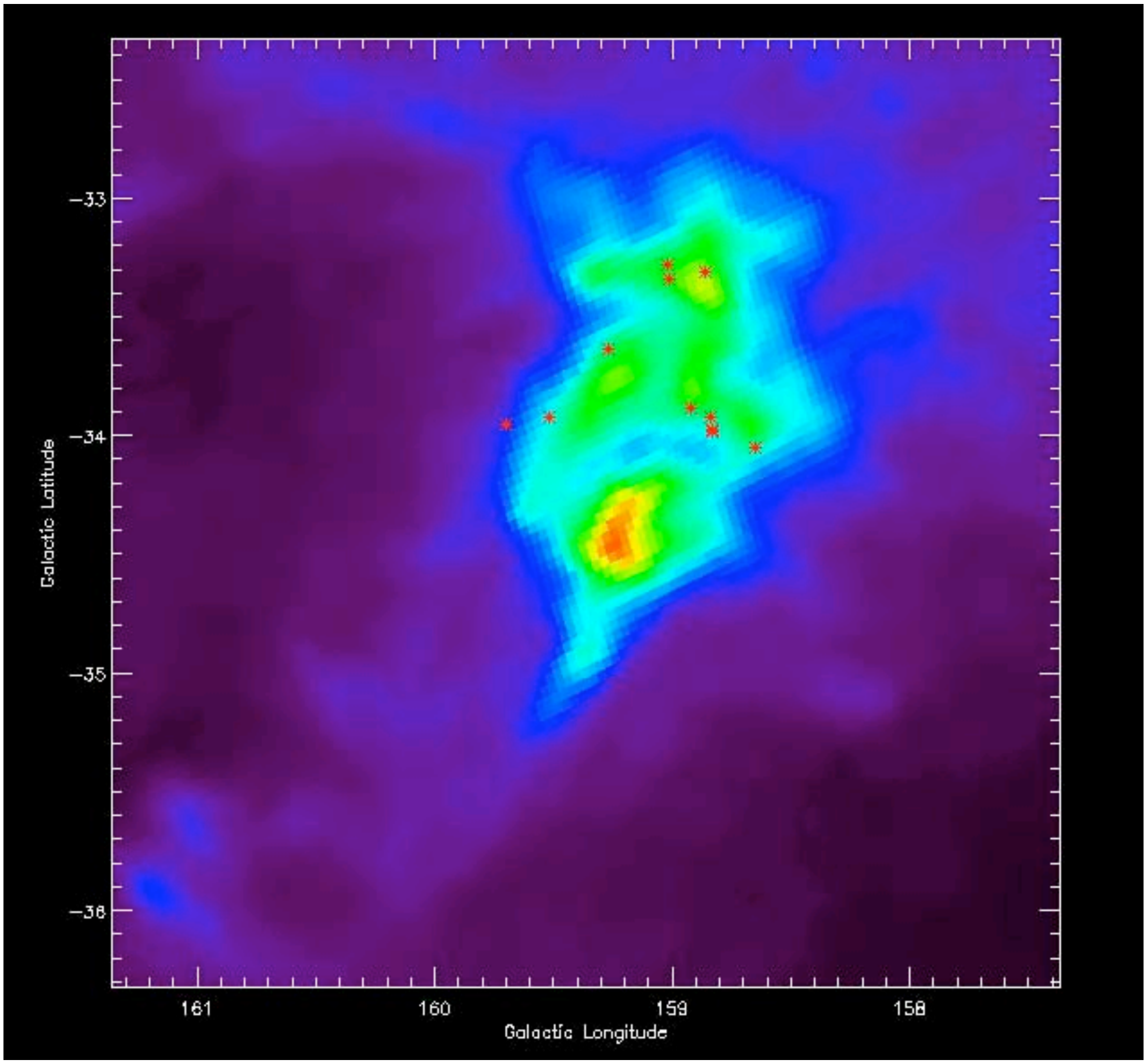

Figure 2-3. Positions of known YSOs from Luhman (2001) plotted on the color excess map from Schlegel, Finkbeiner, and Davis (1998) as the red asterisks. LkHα 262 and 263 are at virtually the same position and one other YSO is off the map (S18), most likely being associated with MBM 13.

proposed that four more candidates may exist in the region. They were detected by looking for Hα emission using a slitless grism spectrograph on the 2.6 m reflector of Byurakan Astrophysical Observatory, Armenia. These four objects were later shown by Luhman and Steeghs (2004) to be field dwarfs based on the absence of Li (6706Å) absorption in their spectra. Thus, as of this writing, the correct known number of YSOs in MBM 12 is 12 (although one object is probably associated with the nearby cloud, MBM 13). On this basis, we can conclude that during the past 10 million years, MBM 12 has given rise to a young T-association. Is the current census of the T-association complete and is there a younger generation of stars forming in the cloud? We will present a catalog of candidates in this thesis that should prove useful in answering these questions.

2.3 Purpose of Spitzer Observations

The Spitzer Space Telescope (described in section 3.1) has been extremely useful in the discovery of new YSOs in many various regions of the sky, for example, the Trifid Nebula (Rho et al. 2006), the Serpens dark cloud (Harvey et al. 2006), the Perseus molecular cloud complex (Jørgensen et al. 2006), and the N63 and N180 HII regions of the Large Magellanic Cloud (Caulet et al. 2008). The results presented in these papers have shown that Spitzer photometry can clearly identify protostars unseen by other methods or instruments. With this in mind, we asked the question, are the 12 known YSOs in MBM 12 the only ones that have formed in the cloud? With high-resolution Spitzer data, we hope to identify all young stellar candidates in the region. With this catalog of potential YSOs, follow-up optical observations can determine how many of these candidates are actually YSOs. Once this is done, the complete census of YSOs in this cloud can be made and, if Class 0/I objects are present, a temporal star formation history of the cloud can be determined. Combining this result with the most recent mass estimates, we can then determine the star formation rate of this dark/translucent molecular cloud.

Chapter 3: The Spitzer Space Telescope

3.1 The Telescope and Instruments

The Spitzer space telescope is an infrared space observatory and is one of the four instruments of the Great Observatories NASA program[7]. It was launched in August of 2003 destined to be the most advanced infrared observatory to date. The spacecraft carries an 85-centimeter telescope and its scientific payload consists of three cryogenically-cooled instruments capable of performing imaging and spectroscopy from the near to the far infrared. The three instruments aboard the observatory are the Infrared Array Camera (IRAC: Fazio et al. 2004), the Infrared Spectrograph (IRS; Houck et al. 2004), and the Multi-band Imaging Photometer for Spitzer (MIPS; Rieke et al. 2004).

IRAC is capable of imaging at four different wavelengths, 3.6, 4.5, 5.8, and 8 microns. This four-channel camera takes simultaneous 5.2' x 5.2' images. The final IRAC images are mosaicked from 722 of these 5.2' x 5.2' images. The detector arrays are 256 x 256 pixels in size, with pixel sizes being 1.2" x 1.2". Fields of view are imaged in pairs using dichroic beamsplitters (3.6 and 5.8 μm; 4.5 and 8.0 μm). The photometric accuracy of the IRAC data, using the normal Spitzer data pipeline reduction modules is better than 10 %.

The IRS is comprised of four spectrograph modules covering a wavelength range of 5.2 to 38 microns. Two of the modules provide "low" spectral resolution (R ~ 60 – 127) while the

---

[7] The other great observatories are the Hubble Space Telescope (HST), the Compton Gamma Ray Observatory (CGRO), and the Chandra X-ray Observatory (CXO).

other two provide "high" spectral resolution (R ~ 600). The "low" resolution modules span a wavelength range of 5.2 to 38 microns while the "high" resolution modules cover 9.9 to 37.2 microns.

MIPS has imaging capabilities at 24, 70, and 160 microns. The three separate detector arrays have field of views of 5.4' x 5.4' (24 μm), 5.25' x 2.6' (70 μm), 0.53' x 5.33' (160 μm). The final MIPS images are mosaicked from 765 of these individual frames. Pixel sizes for each array are 2.49" x 2.60" (24 μm), 9.85" x 10.06" (70 μm), and 15.96" x 18.04" (160 μm). The photometric accuracy of the MIPS data is better than 10 %.

For our observations, we took advantage of the photographic capabilities of IRAC and MIPS. More information on the abilities of each of these instruments can be found at http://ssc.spitzer.caltech.edu/irac/ and http://ssc.spitzer.caltech.edu/mips/ respectively.

3.2 The Images

MBM 12 was observed with the Infrared Array Camera at 3.6, 4.5, 5.8 and 8.0 μm on four separate dates to ensure complete coverage of the molecular cloud region (~3.5 square degrees). In addition to improving the signal to noise ratio, this method is also employed to "weed out" transitory objects such as asteroids and comets. The region was observed on 2006 September 23, 2007 February 17, 2007 February 20, and 2007 September 11 (Spitzer AOR[8] keys 0018148608, 0018149120, 0018148864, and 0018149376, respectively). Observations took, on average, two hours and fifty-five minutes each for a total of 41.918 kiloseconds of observing time and encapsulated approximately 3.5 square degrees of sky coverage. MBM 12

[8] An Astronomical Observation Request (AOR) is the sequence of observations made for a particular investigators program.

was also observed with the Multi-band Imaging Photometer for Spitzer at 24, 70, and 160 μm on three separate occasions. These observations took place on 2007 September 17 to September 18, and twice on 23 September 2007 (Spitzer AOR keys 0018149888, 0018149632, and 0018150144 respectively). Observations took, on average, two hours and forty-three minutes each for a total of 29.389 kiloseconds of observing time and covered approximately 3 square degrees of sky. The images are presented in Figures 3-1 through 3-11. One of the most informative images is Figure 3-10 which shows the three-color combined IRAC images along with CO(1-0) contours. The image shows some potentially interesting correlations (or anticorrelations) between the infrared emitting dust and the molecular gas. Regions of anticorrelation are proposed to be due to the decrease of polycyclic aromatic hydrocarbons in dense gas regions. The data reduction techniques are discussed in Chapter 4.

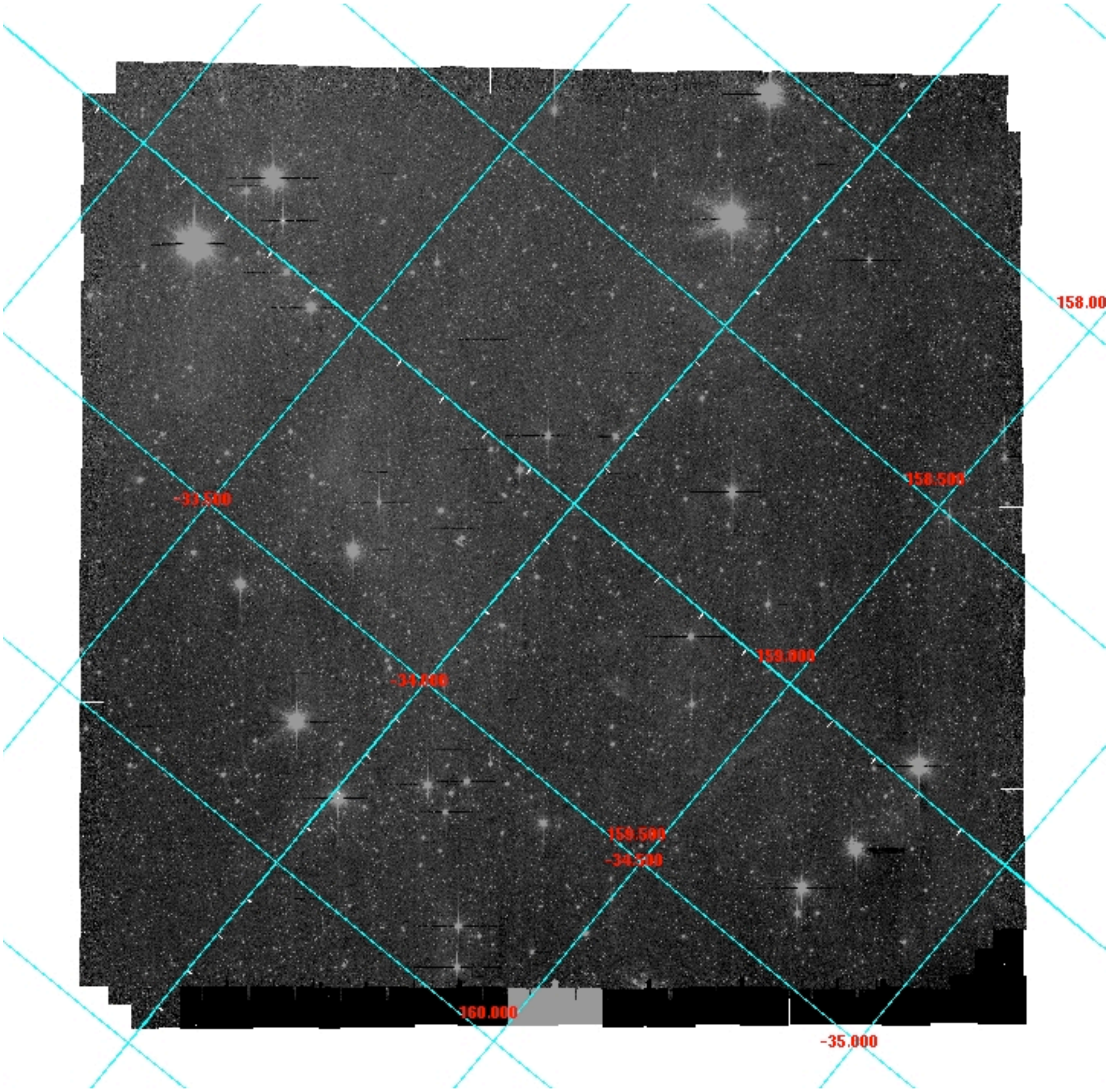

Figure 3-1. Template coordinate grid in *l* and *b* for Figures 3-2 through 3-6 and 3-11. The underlying image is the 3.6 μm image from the IRAC instrument, and is shown without the gridlines in the next figure.

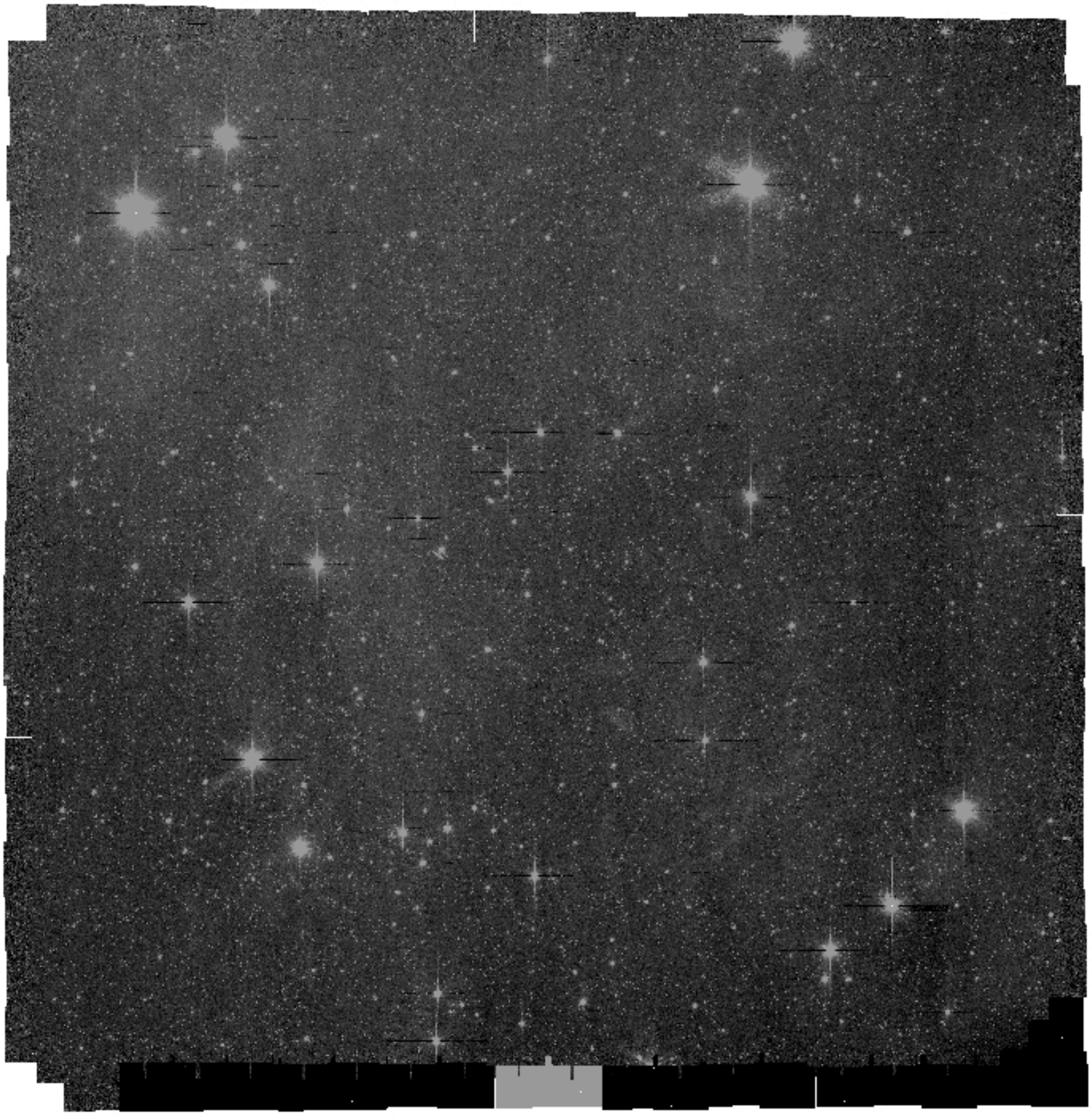

Figure 3-2. 3.6 μm image from the IRAC instrument mosaicked from 722 5.2’ x 5.2’ tiles. Being the nearest of all the observed wavelengths to the optical portion of the electromagnetic spectrum, the 3.6 μm image shows a myriad of point sources that are predominantly stellar in nature.

Figure 3-3. 4.5 μm image from the IRAC instrument. Similar to the 3.6 μm image, many point sources can still be seen.

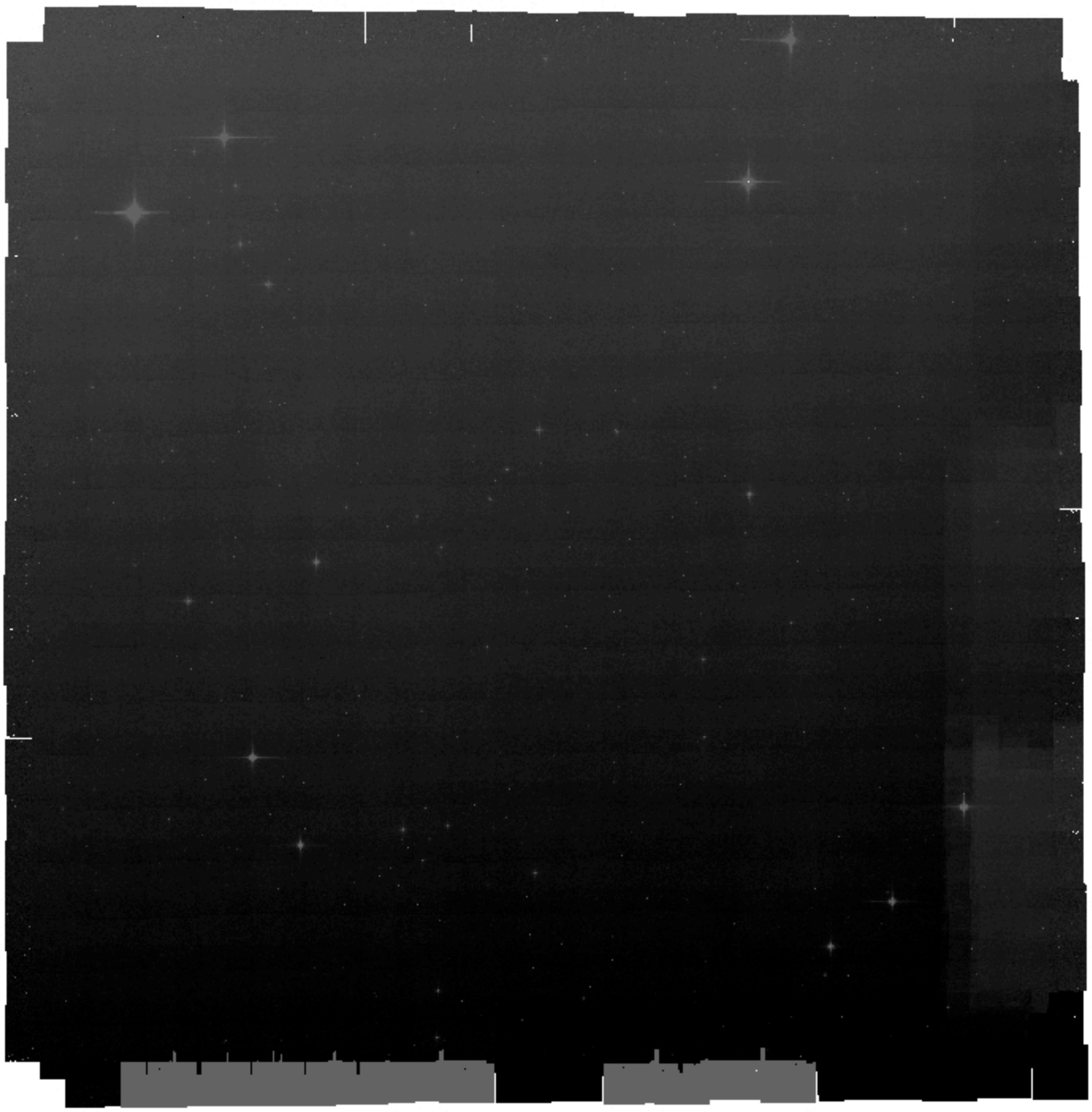

Figure 3-4. 5.8 μm image from the IRAC instrument. Many of the point sources seen in Figures 3-1 and 3-2 no longer emit significantly at the longer wavelengths, as can be seen by comparing this image to the previous two.

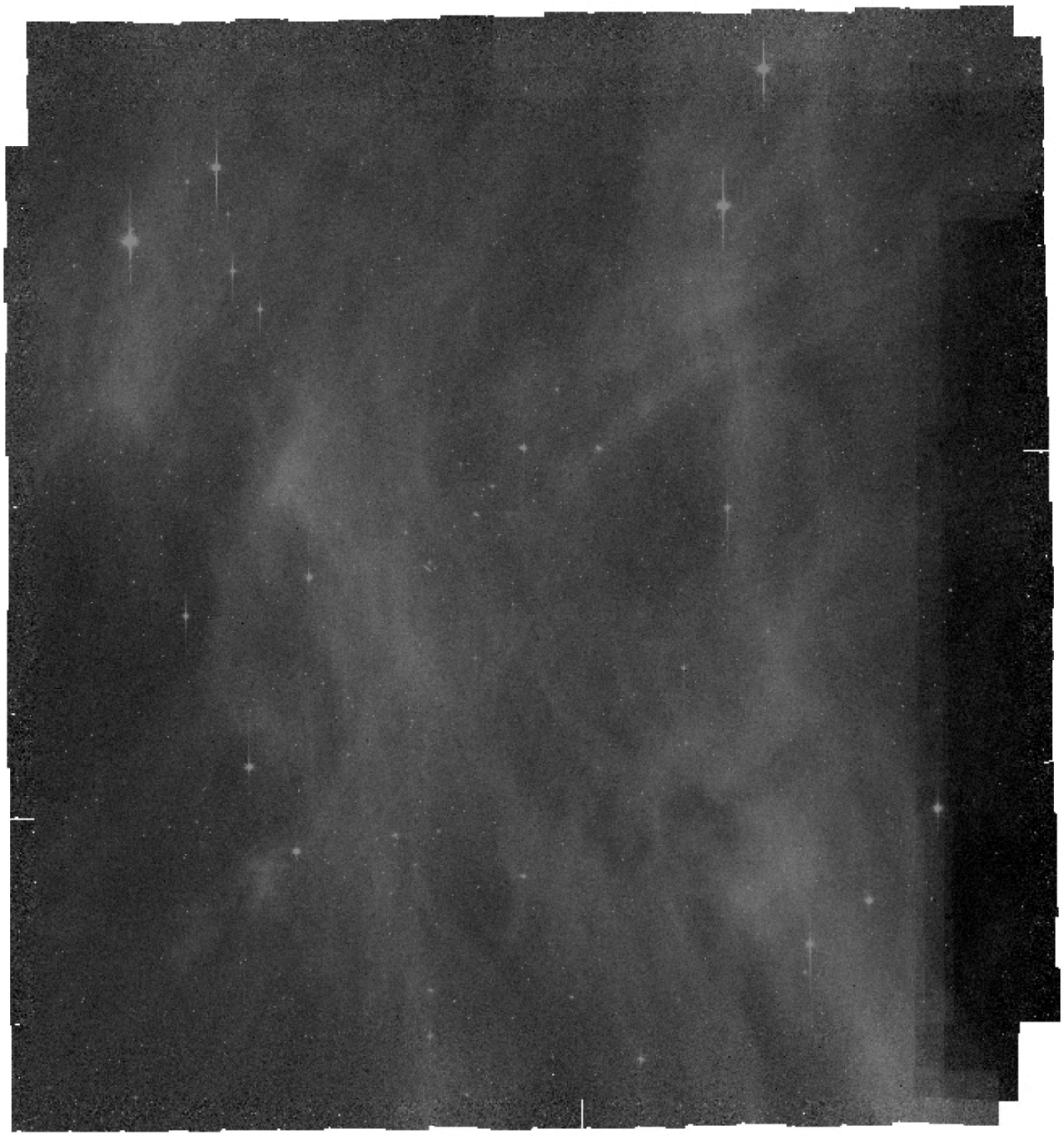

Figure 3-5. 8.0 μm image from the IRAC instrument. Point sources are even less noticeable in this image, although the dust structure of MBM 12 now begins to become prominent.

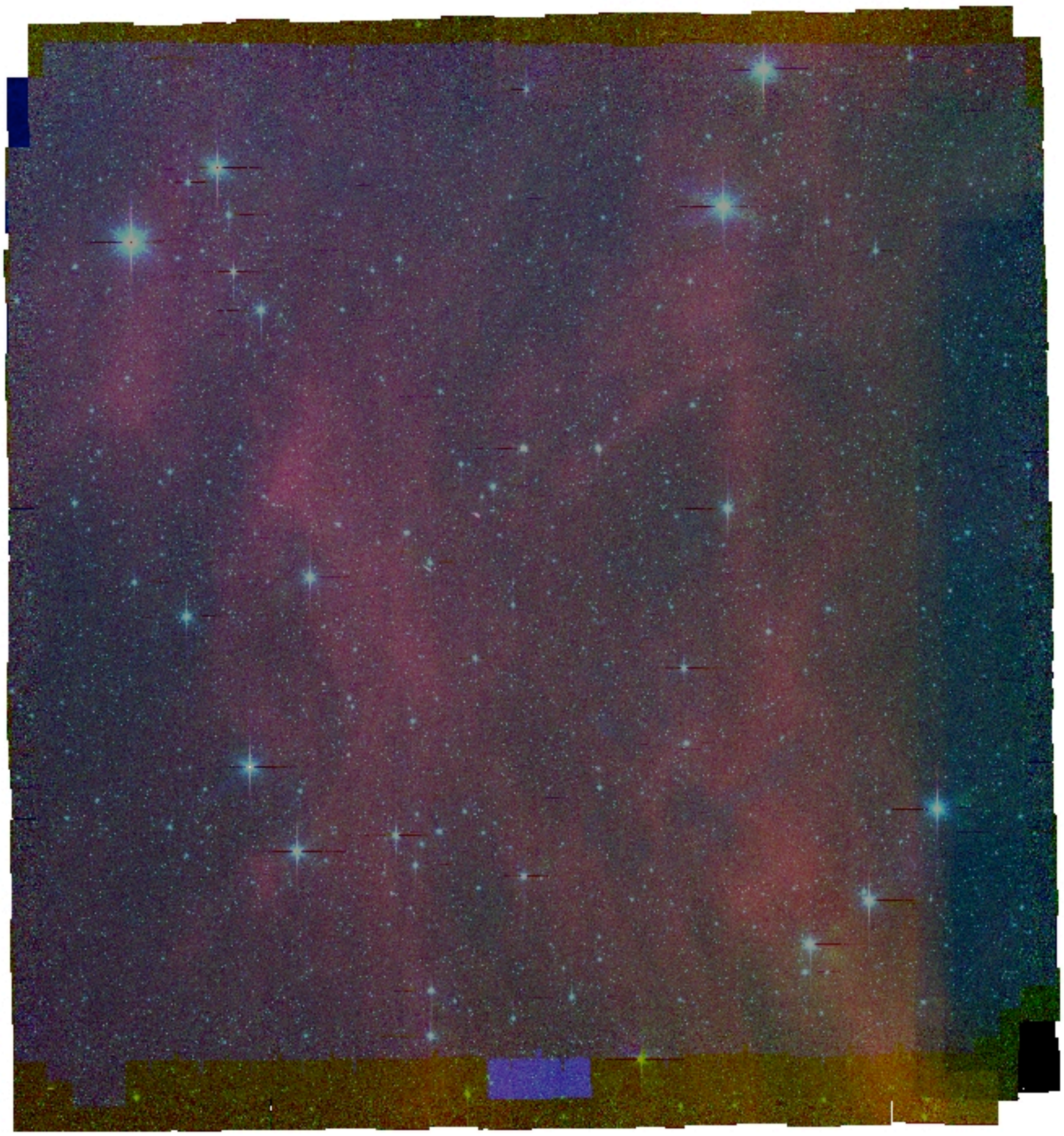

Figure 3-6. A multi-wavelength combined image, with IRAC 3.6 (blue), 4.5 (green) and 8.0 (red) micron images superimposed to make a final image.

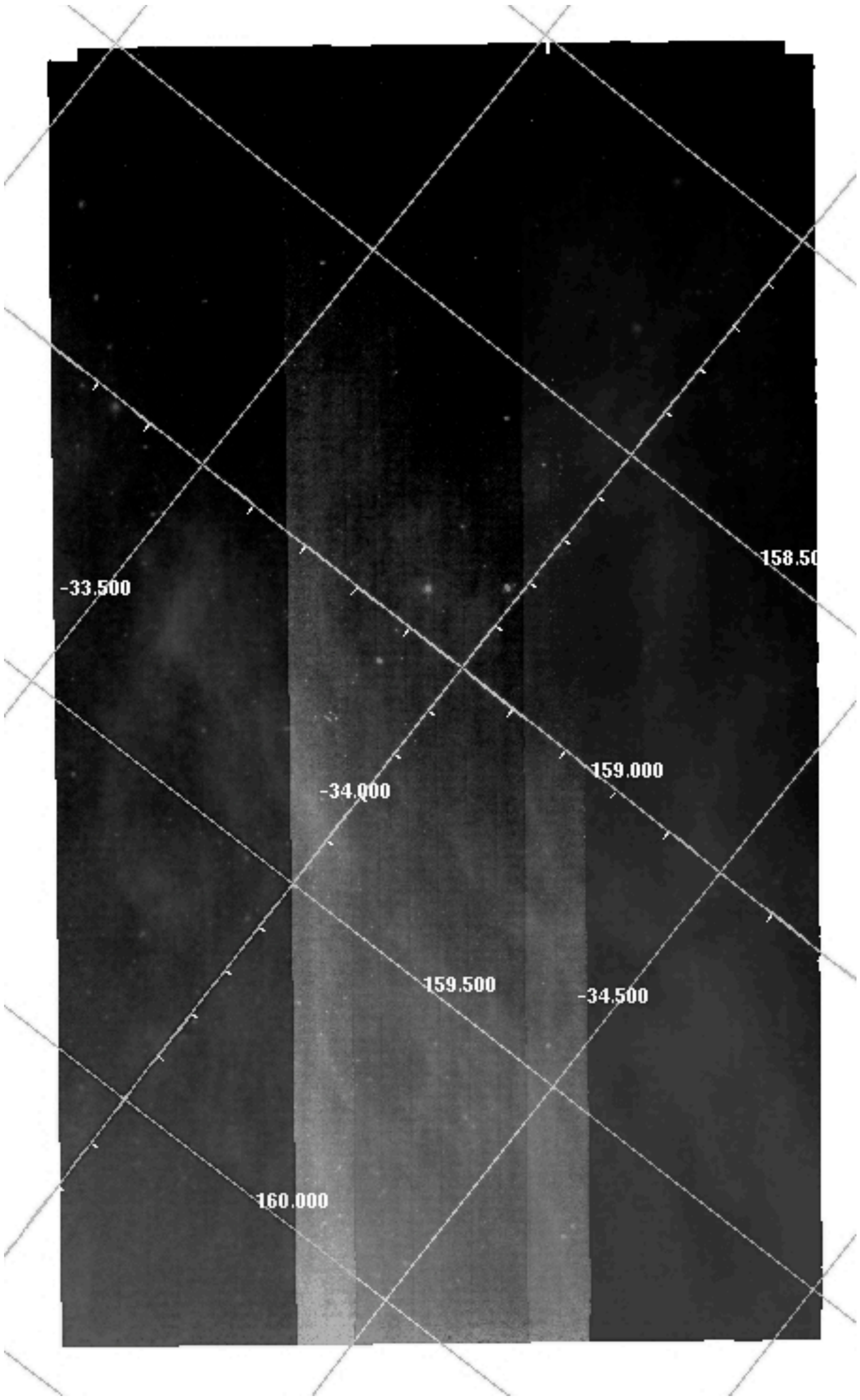

Figure 3-7. Template coordinate grid in *l* and *b* for Figure 3-8. The underlying image is at 24 μm and is shown without the gridlines in the next figure.

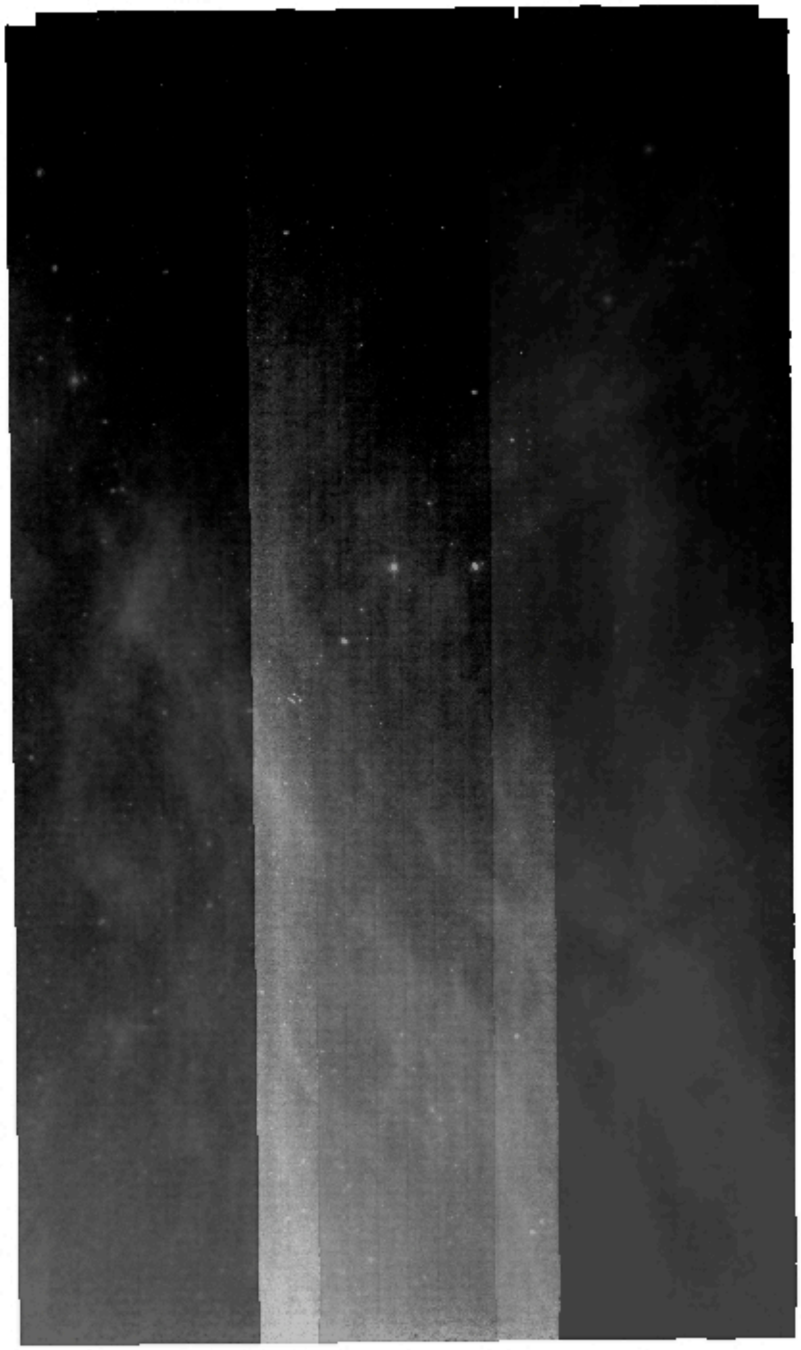

Figure 3-8. 24 μm image from the MIPS instrument. Image shows the mixture of cloud structure and point sources.

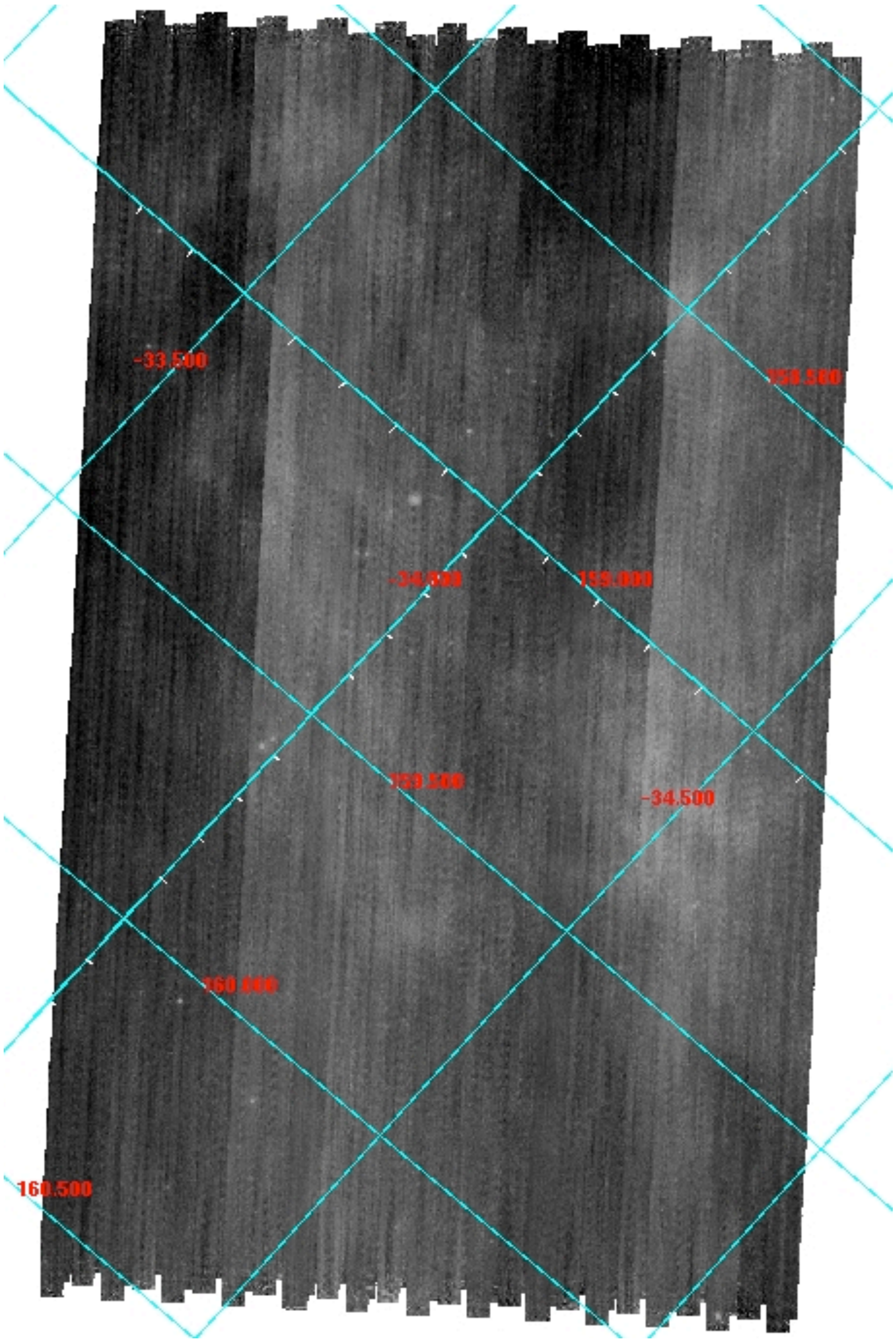

Figure 3-9. Template coordinate grid in *l* and *b* for Figure 3-10. The underlying image is at 70 μm and is shown without the gridlines in the next figure.

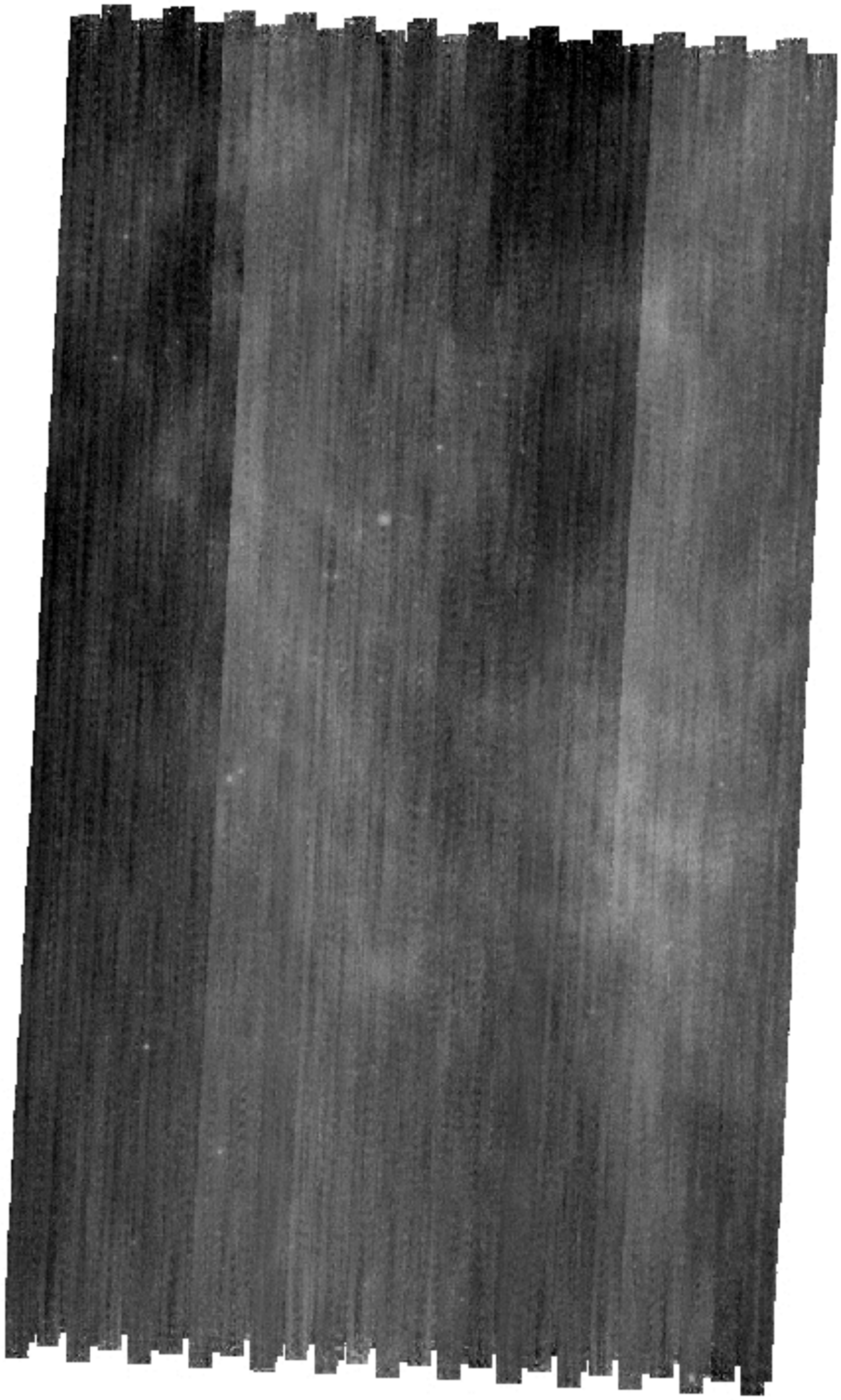

Figure 3-10. 70 μm image from the MIPS instrument. Although many artifacts can be seen, the filamentary structure of MBM 12 is evident, as well a many of the brighter infrared point sources.

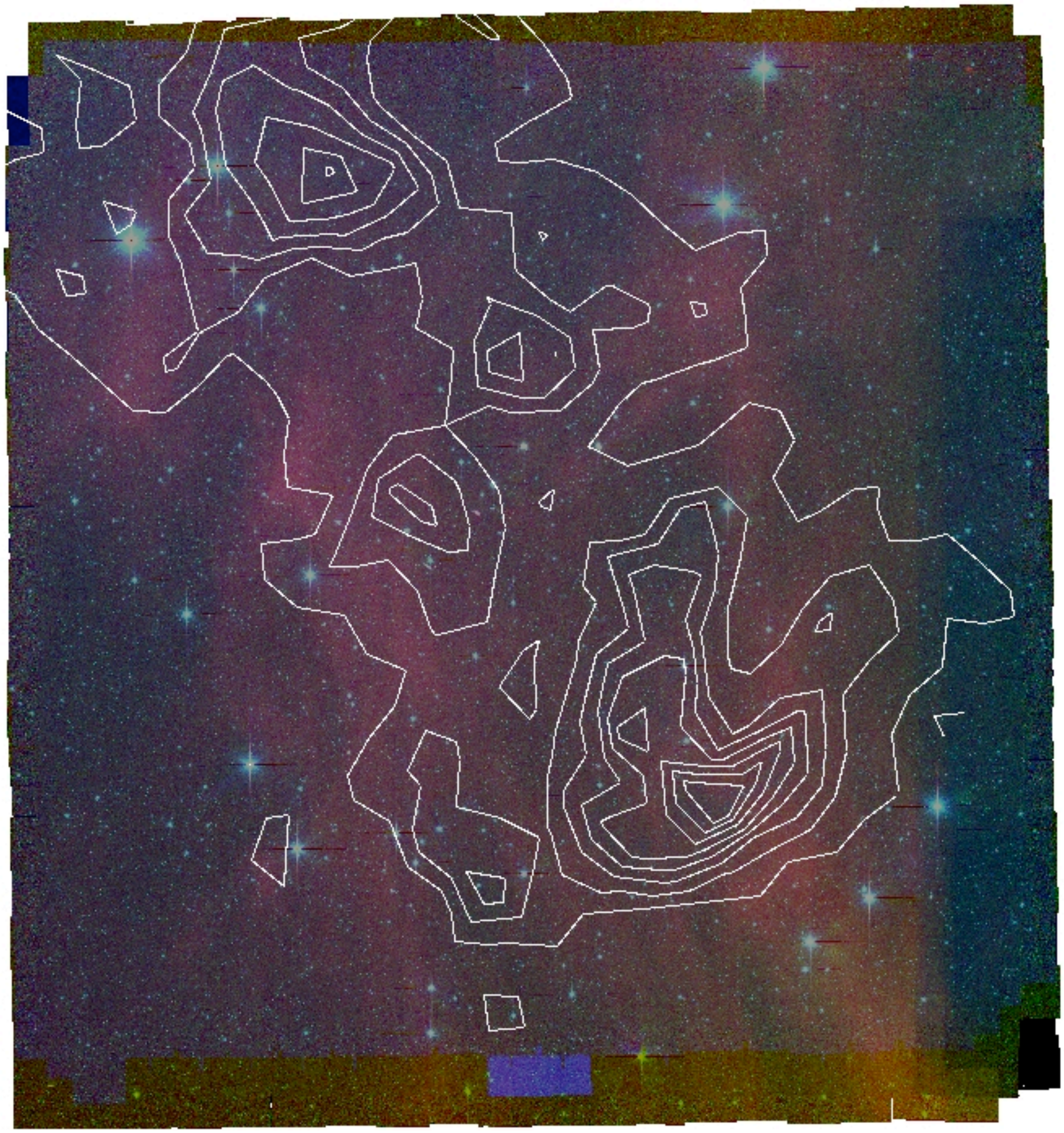

Figure 3-11. A contour map was made from the CO(1-0) map shown in figure 2-2 and superimposed onto the three-color map from IRAC. Interesting to note is the apparent anticorrelation of dust and CO emission in some areas such as the 'horseshoe' located in the lower right portion of the image. The reason for this is thought to be the decrease in polycyclic aromatic hydrocarbons (PAHs) in dense gas regions.

Chapter 4: The YSO Catalogs

4.1 Data Analysis

The IRAC and MIPS images were retrieved from the Spitzer archive after the data were made available using the Leopard software developed by the Spitzer Science team. The data downloaded include the raw data, basic calibrated data (BCDs), and post-BCD data. The raw images are the original FITS[9] files of the data. The BCDs are the individual frames with permanently damaged pixels and pixels affected by cosmic-rays removed. Post-BCD data products include the mosaicked images for each channel on each observation date. Because the Spitzer Instrument and Instrument Support Teams are constantly updating, revising, and improving data processing pipelines, images retrieved were processed with different pipelines depending on the date the data were taken. These data processing pipelines are devised by the team at the Spitzer Science Center (SSC) on the campus of Caltech in Pasedena on all AORs and then released to the principle investigators and, eventually, the general public. Information on what corrections or improvements were made for each pipeline can be found at http://ssc.spitzer.caltech.edu/archanaly/plhistory/. The IRAC data from 23 September 2006 was processed with the S14.4.0 pipeline. The IRAC data from 20 and 23 February 2007 were processed with the S15.3.0 pipeline. The rest of the IRAC and MIPS data were processed with the S16.1.1 pipeline. The Spitzer Science Center (SSC) also provides post-BCD tools such as the Mosaicker and Point source Extractor (MOPEX). MOPEX can be used to produce

[9] Flexible Image Transport System is the standard astronomical image and header format.

mosaicked images of individual BCD frames. MOPEX also includes a point source extraction package called APEX. APEX works by identifying contiguous clusters of pixels with values greater than a specified threshold. After combining these images, we were ready to analyze them for YSOs.

4.2 The 70 μm Catalog

Many methods can be used to identify YSOs with Spitzer data. We choose to employ multiple methods of investigation, thereby attaining a high level of discrimination by finding those sources that are identified by two or more techniques. This will ensure that the resulting catalogs of potential YSOs include the most promising candidates.

As an initial first look survey of the received data, a visually selected sample of the brightest sources seen in the 70 μm image were recorded. The candidates were selected by visual inspection of the image because the most deeply embedded objects emit strongly at longer wavelengths. Regular point source extraction was not performed because the image contains too many artifacts to create a reliable source list. A list compiled based on this criterion comprised 79 sources. Eighteen of these sources were discarded because either they were not seen in any other waveband (implying they could possibly be asteroids), or the area of the 70 μm image where they were detected did not overlap with the area of the other image's wavebands. The remaining 61 sources are listed in Table 4-1. These sources were cross-referenced with the known YSOs residing in MBM 12 from Luhman (2001), with sources known to exist in the Sloan Digital Sky Survey (SDSS), and with the SIMBAD astronomical database. Sloan data can be used to determine if a source is stellar or extragalactic in nature. Other names and Sloan designations are also shown in Table 4-1. In the case of #20, two Sloan sources were detected

Table 4-1

70 µm Sample Sources

ID	α(2000)	δ(2000)	Name[10] or Sloan Designation
1	02 57 58.01	20 40 29.7	…
2	02 58 11.23	20 30 03.5	E 0255.3+2018
3	02 58 26.14	20 20 02.3	…
4	02 58 06.41	20 19 32.8	Star
5	02 56 23.89	20 25 18.1	Galaxy
6	02 57 19.19	20 30 10.3	Star
7	02 56 05.89	20 23 51.9	…
8	02 53 53.61	20 26 58.5	Galaxy
9	02 57 26.64	19 56 54.0	Galaxy
10	02 57 00.41	19 52 46.7	Galaxy
11	02 57 03.95	20 00 44.0	IRAS 02542+1948
12	02 56 37.56	20 05 37.1	Lkhα 264
13	02 56 44.42	20 14 53.5	…
14	02 56 17.53	20 10 06.2	Galaxy
15	02 56 07.99	20 03 24.3	Lkhα 262
16	02 56 08.42	20 03 38.6	Lkhα 263
17	02 55 27.65	19 31 05.8	Galaxy
18	02 56 18.59	19 23 27.2	…
19	02 57 19.92	19 47 11.7	Galaxy
20	02 57 59.58	19 47 28.7	Galaxy/Star?
21	02 58 18.48	19 42 30.9	Galaxy
22	02 58 22.73	19 42 03.3	Galaxy
23	02 59 30.29	19 40 03.2	Galaxy
24	02 59 16.72	19 21 17.6	…
25	02 58 59.99	19 10 48.7	Galaxy
26	02 56 01.74	19 18 33.6	…
27	02 54 49.86	20 22 22.3	HD 18066
28	02 55 24.90	19 54 21.9	TYC 1227-287-1
29	02 55 33.71	20 13 33.1	Galaxy
30	02 56 34.62	19 14 47.6	Galaxy
31	02 55 40.84	20 32 58.3	Galaxy
32	02 57 13.97	20 00 10.1	…
33	02 56 55.61	20 00 20.3	Galaxy
34	02 57 41.52	19 50 22.8	Galaxy
35	02 57 29.64	19 57 09.0	2MFGC 2400
36	02 57 23.97	19 17 45.5	Galaxy
37	02 58 04.45	19 14 36.9	…

[10] From Luhman (2001) or SIMBAD

38	02 58 13.05	19 20 22.5	Galaxy
39	02 57 26.85	20 39 09.4	…
40	02 58 29.72	20 27 48.7	…
41	02 58 59.19	20 07 41.1	Galaxy
42	02 58 16.09	19 47 19.6	RX J0258.3+1947
43	02 59 44.04	19 31 53.7	2MASX J02594426+1931566
44	02 59 48.74	19 25 37.7	Galaxy
45	02 59 20.29	19 28 39.5	Galaxy
46	02 59 29.73	19 25 44.5	Star
47	02 54 18.73	20 23 31.3	Galaxy
48	02 54 23.03	20 23 46.5	Galaxy
49	02 54 25.22	20 08 31.7	…
50	02 54 27.78	20 08 17.8	Galaxy
51	02 54 26.41	20 18 59.7	…
52	02 54 45.20	20 17 12.6	…
53	02 56 26.76	20 17 52.2	…
54	02 57 01.15	20 05 40.3	…
55	02 57 55.01	19 42 50.2	Star
56	02 56 34.74	20 03 18.3	Galaxy
57	02 59 45.27	19 18 51.2	…
58	02 57 50.66	19 48 02.2	Star
59	02 57 38.01	19 41 28.5	Galaxy
60	02 55 49.07	19 56 06.7	Galaxy
61	02 54 37.54	19 59 22.3	Star

within 1 arcsecond of the position selected, one a star and the other a galaxy. As seen in the table, many of these sources (at least 30 of the 61) are known to be background galaxies. Infrared emission at 70 μm is a good tracer of dust rich galaxies (Sanders and Mirabel 1996). Only 13 of the sources are known to be stars, five of them being known YSOs in MBM 12 from Luhman (2001), leaving 17 sources of unidentified origin. The remaining 6 known YSOs that were not seen in this sample are most likely not detected because they may be Class III YSOs[11], which do not emit strongly at longer infrared wavelengths. The analysis of these sources will be discussed further in chapter 5.

4.3 The 8 μm Catalog

Our next method of YSO detection started with a new source catalog. The MOPEX data reduction package includes a point source extraction program named APEX (described above in Section 4.1). Source detection was performed on the 8 μm IRAC mosaic to be used as a primary list of protostar candidates. This selection of sources was designed to eliminate a large number of background stars that would be picked up in the more sensitive 3.6 and 4.5 μm bands. This extraction resulted in a list of 12,700 sources. The centroids of each of these sources were established by providing the coordinates of each source to the IDL Astronomy Library procedure *cntrd*. This routine determines the centroid of a point source by locating the position where the derivatives in the X and Y directions go to zero. Using the centroid positions, aperture photometry was then performed using the IDL Astronomy Library procedure *aper* (Landsman 1993). Using the *aper* routine, the flux of each of the 12,700 point sources was determined for the 3.6, 4.5, 5.8, 8.0, and 24 μm wavebands. Aperture corrections were employed to scale the

[11] Recall that, of the 12 known YSOs, only 11 are within the field of view of our Spitzer observations.

photometry, necessary due to account for the fraction of light included in the measurement aperture and lost in the background aperture (Reach et al. 2005). The corrections used were 1.049, 1.05, 1.06, 1.068, and 1.175 for the 3.6, 4.5, 5.8, 8.0, and the 24 μm wavebands, respectively. In order to then convert the fluxes to magnitudes, zero-point fluxes were applied. These values are the fluxes that would be measured for a star of zero magnitude. In the same wavelength order as above, the zero-point fluxes were 280.9, 179.7, 115.0, 64.1, and 7.14 (Reach et al. 2005). The positions of these sources were then cross-referenced with the Two Micron All Sky Survey (2MASS) and the Sloan Digital Sky Survey (SDSS) to locate near infrared and optical counterparts. 2MASS can provide data from the J (1.25 μm), H (1.65 μm), and K (2.17 μm) wavebands. SDSS can contribute data from the U (0.3551 μm), G (0.4686 μm), R (0.6165 μm), I (0.7481 μm), and Z (0.8931 μm) wavebands. Matches were selected to be within one arcsecond of the objects' centroid positions.

Of the 12,700 objects found in the 8 μm IRAC image, 3680 were identified by 2MASS (28.97%), and 4829 were identified by SDSS (38.02%). Of the SDSS identifications, 2642 were classified as stellar in nature (54.71% of the Sloan sample; 20.8% of the original list) and 2187 were classified as galaxies (45.29% of the Sloan sample; 17.22% of the original list). Those classified as stellar in nature by Sloan data could still potentially be YSOs, so are not ruled out as candidates. Not all objects detected with the 8 μm sample were detected in the other three wavebands. To select the highest quality sources to be examined for YSO candidacy, we considered only those objects detected in all four wavebands of IRAC. Of the 12,700 objects listed by APEX, 357 (2.81%) were discarded because no flux was detected in any of the four wavelengths, possibly due to oversaturation or false identification of a source (no source at designated position), leaving a total of 12,343. Of the remaining sources, 276 (2.17%) were only detected at one wavelength, 886 (6.98%) were detected at two wavelengths, and 1963 (15.46%) were detected at three wavelengths. This leaves 9,218 objects detected at all four IRAC wavebands. Of these, 549 (5.96%) were revealed to be duplications (two detections at the exact same position), leaving 8,669 sources to be included in the first pass of our high-quality catalog. Within this high-quality catalog, 2,435 (28.09%) sources are known to be stars, and 1,787 (20.61%) are known to be galaxies from identification markers designated by the Sloan database. This leaves 4,447 (51.30%) sources of unknown designation. These data are summarized in Table 4-2 and Table 4-3.

In order to identify potential YSOs with our 8 μm sample, we used an entirely different method than that of the 70 μm sample. Many YSO detecting schemes are based on employing only IRAC magnitudes, or the combination of IRAC and MIPS magnitudes (e.g., Allen et al. 2004, Rho et al. 2006, Hartmann et al. 2005, and Harvey et al. 2006). Color-color and color-magnitude diagrams are especially useful in constraining the characteristic colors of YSOs, thereby separating them from stars and background galaxies contaminating the sample. In order to narrow down the best YSO candidates from our high-quality sample, we have chosen to implement multiple classification techniques. By combining constraints on multiple color-color and color-magnitude combinations, we hope to select the most probable YSO candidates.

The first criterion we will use to select YSO candidates from the 8 μm sample is one that takes advantage of the [8.0] vs. [4.5] - [8.0] color-magnitude diagram. This method, first used by Harvey et al. (2006) has two statistical requirements for choosing candidates. They are (1) $[4.5] - [8.0] > 0.5$ magnitudes and (2) $[8.0] < 14$ mag. $- ([4.5] - [8.0])$. By comparing their sample of sources from the Serpens dark cloud to an off-cloud region and a subset of Spitzer Wide-area Infrared Extragalactic Survey (SWIRE) data, they show the existence of two distinct regions

Table 4-2

8 μm Sample

Detections	Number	Percentage
None	357	2.81
In One Band	276	2.17
In Two Bands	886	6.98
In Three Bands	1963	15.46
In All Four Bands	9218	72.58

Table 4-3

High Quality Catalog

Type	Number	Percentage
Stars	2,435	28.09
Galaxies	1,787	20.61
Unknowns	4,447	51.30

characterizing stellar and extragalactic sources. The overwhelming majority of stellar sources were shown to have [4.5] – [8.0] colors less than 0.5 magnitudes because of their lack of infrared excess and the majority of extragalactic sources had [8.0] magnitudes fainter than 14 – ([4.5] – [8.0]). This behavior is possibly due to the heated dust produced by active star-forming regions occurring in many of these extragalactic sources. Figure 4-1 shows the color-magnitude plot for all members of the high-quality catalog with the inclusion of the boundaries defining the candidate YSO region described above. As can clearly be seen in Figure 4-1, these constraints separate the bulk of stars and extragalactic sources from candidate YSOs. Of the known YSOs, the 5 Class II sources are clearly within this region. To further illustrate the effectiveness of this selection technique, individual plots of known stars and known galaxies are shown in Figure 4-3. One hundred and seventy-four sources from the high-quality catalog met the selection criteria. Of these, from comparison to SDSS sources, 54 (31.0%) are known to be stars, 61 (35.1%) are known to be galaxies, and 59 (33.9%) have unknown designations. This method gives 113 sources as YSO candidates either known to be stars or of unknown classification. These sources are organized in Table 4-4 with magnitudes from SDSS, 2MASS, IRAC and MIPS tabulated when available.

To further constrain this population of candidates into probable YSO types (0,I,II,III), we implement two color – color diagram schemes. The first classification system was originally devised by Allen et al. (2004) and utilizes the IRAC [3.6] – [4.5] and [5.8] – [8.0] colors. This diagram is shown in Figure 4-4. This method divides sources into three separate areas corresponding to different YSO Classes. The Class II YSO region is defined by [5.8] – [8.0] colors between 0.4 and 1.1, and [3.6] – [4.5] colors between 0.0 and 0.8. The Class I/II region is

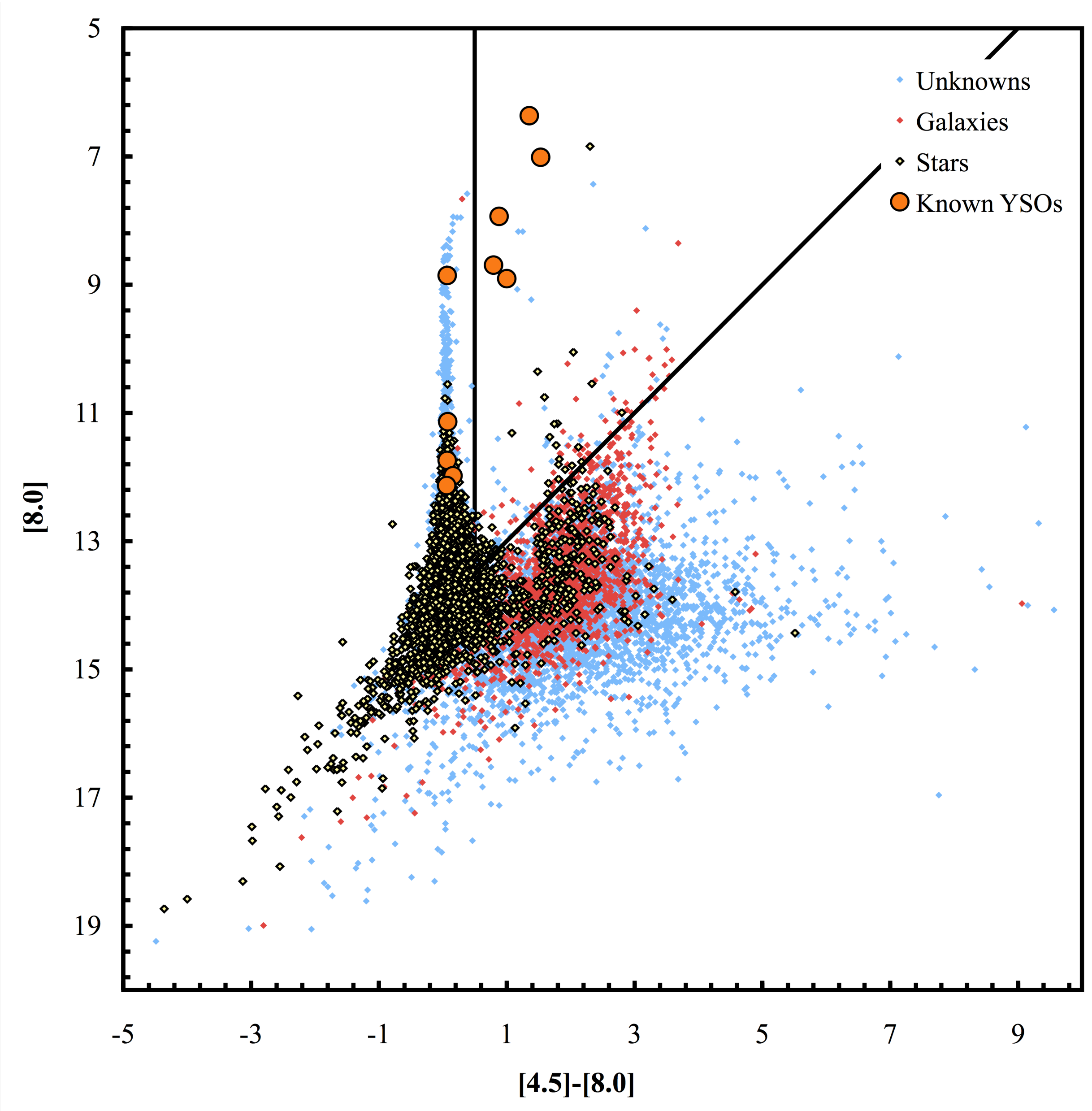

Figure 4-1. Color – magnitude diagram for entire high-quality catalog. For comparison, the known YSOs that reside in MBM 12 are plotted. Although some of the known YSOs fall in the color region [4.5] – [8.0] less than 0.5, putting them in the normal star regime (likely Class III), the remainder do fit into the restrictions placed on finding new YSO candidates. Photometric uncertainties for the magnitudes are in the 5-10% range.

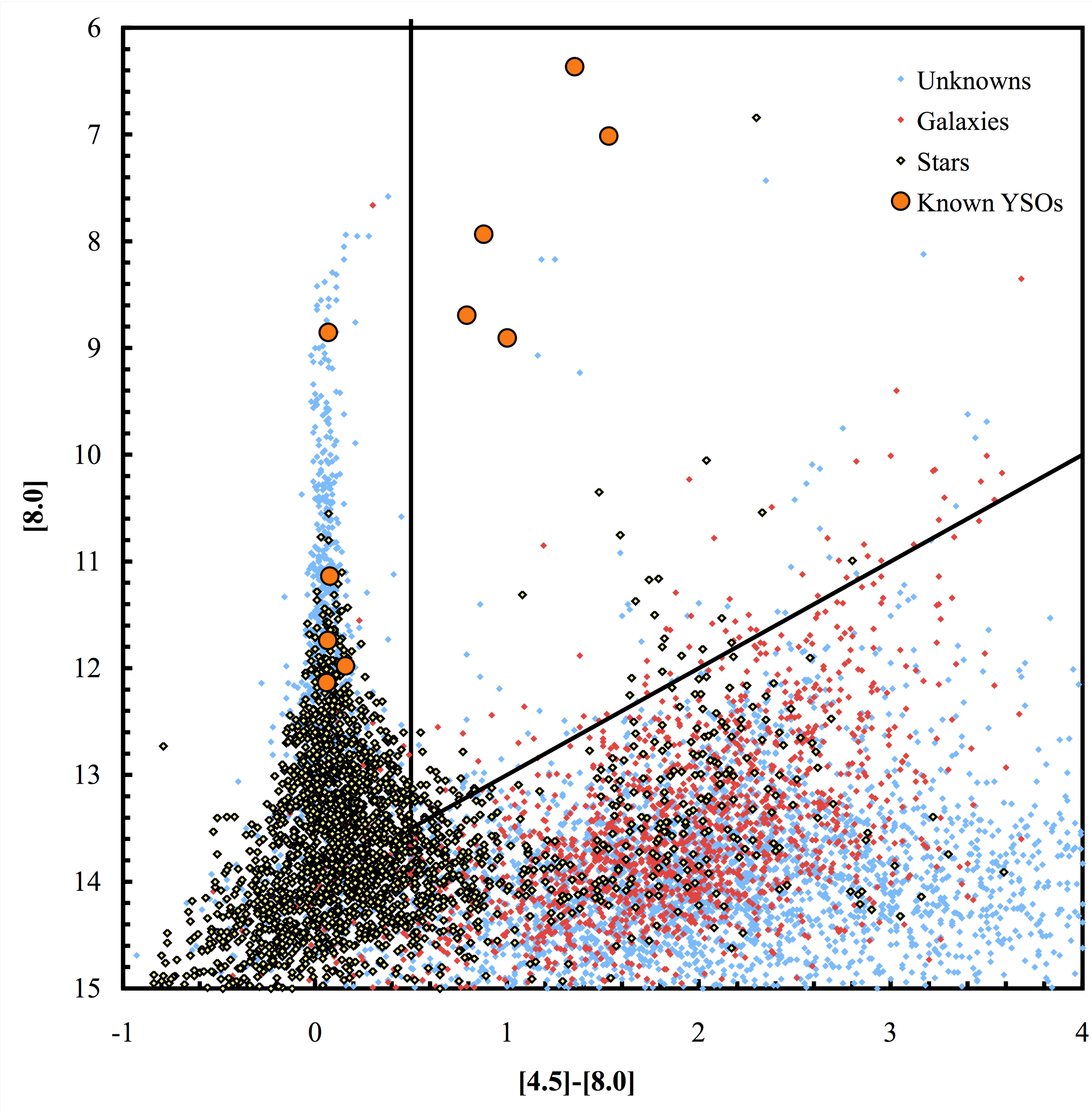

Figure 4-2. Close-up of YSO classification region from Figure 4-1.

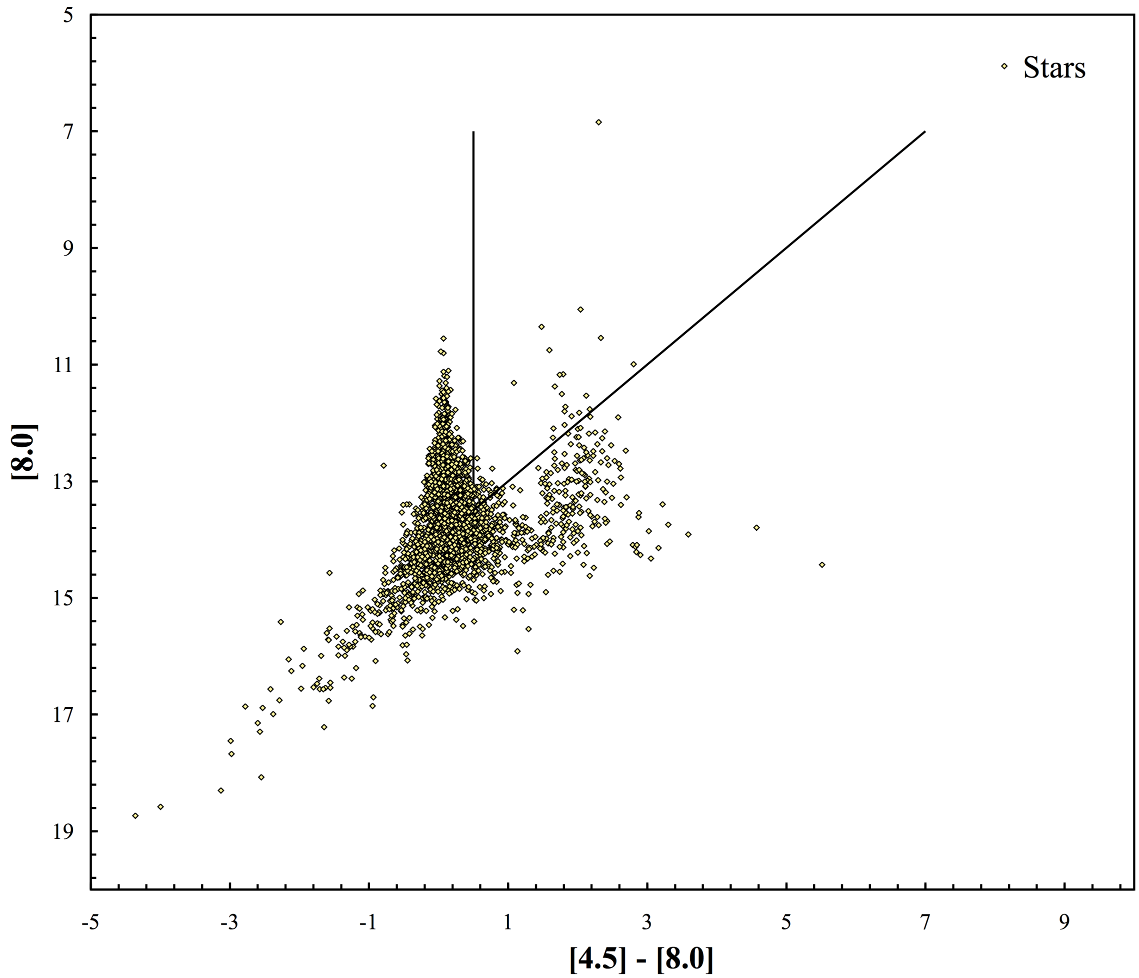

Figure 4-3a. Color – magnitude diagrams for stars and galaxies from high-quality catalog. This figure shows the loci of the objects identified by the Sloan database as stars. The lines designate the candidate YSO region.

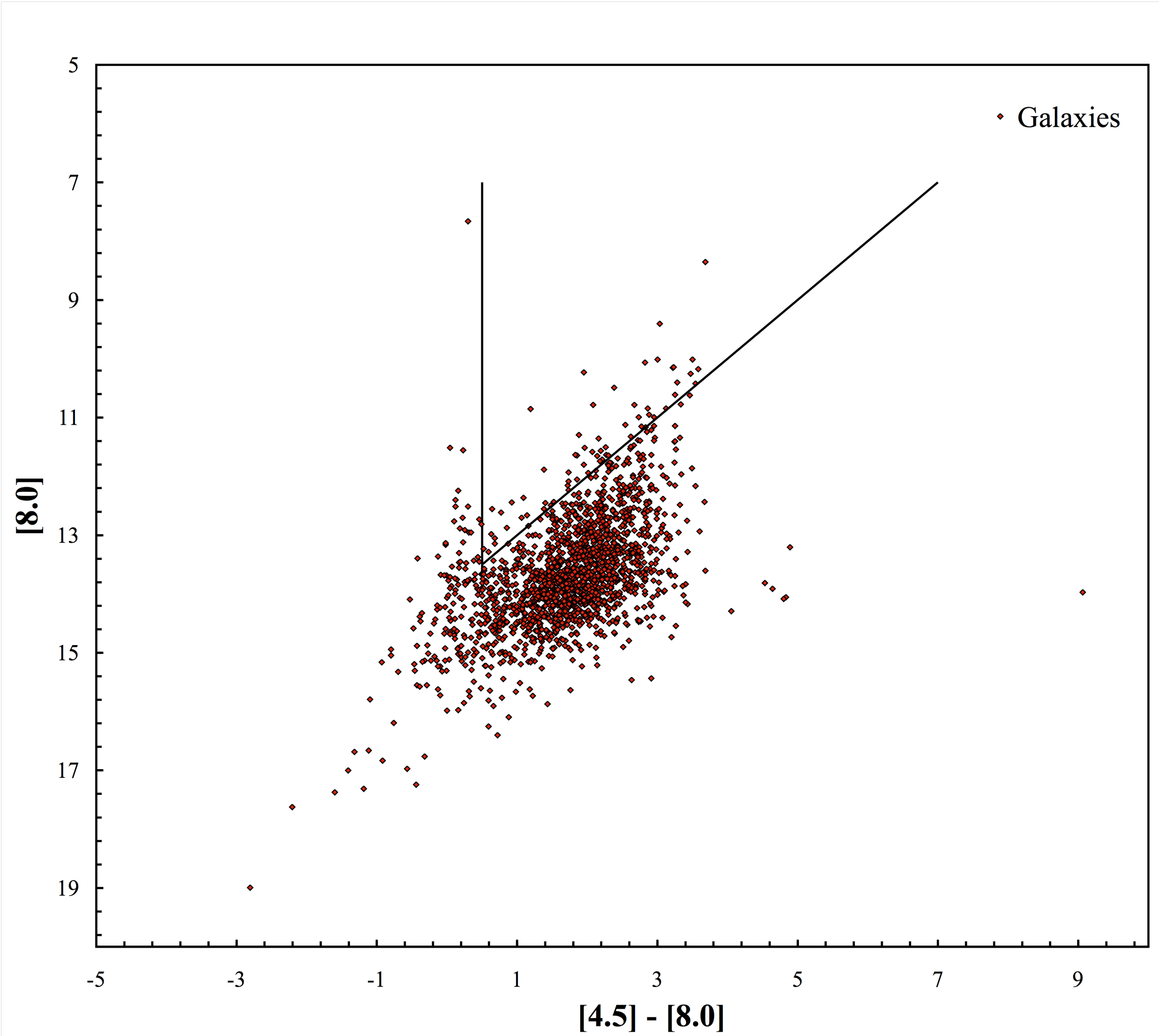

Figure 4-3b. Same as Figure 4-4a, but with objects designated as extragalactic by the Sloan database.

Table 4-4
8 μm IRAC Sample Candidates

ID	α(2000)	δ(2000)	U	G	R	I	Z[a]	J	H	K[b]	3.6	4.5	5.8	8	24[c]
1	44°.64899	19°.16544	17.953	16.312	15.564	15.183	14.969	13.984	13.519	13.412	13.31	13.34	12.71	12.78	11.38
2	45.13427	19.338802	19.217	18.938	18.77	18.999	18.834	...	...	...	14.55	13.74	12.91	12.09	...
3	45.043179	19.340622	18.587	16.732	15.975	15.666	15.441	14.408	13.881	13.786	13.68	13.76	13.71	13.19	...
4	44.625526	19.22522	19.475	19.061	18.458	18.267	18.156	...	...	...	13.88	12.87	12.04	10.54	7.7
5	45.055542	19.475325	17.312	16.223	15.581	15.384	15.329	14.434	14.114	14.06	13.97	13.96	14.08	13.39	...
6	44.110836	19.212753	21.032	18.308	16.927	16.341	15.938	14.694	14.05	13.881	13.6	13.55	13.2	12.95	10.58
7	44.873646	19.428909	19.22	18.5	17.959	17.538	17.183	...	...	...	13.66	12.95	12.16	11.16	7.59
8	43.769863	19.117449	25.714	20.993	18.837	17.528	16.715	15.143	14.227	13.91	13.67	13.64	13.13	13.09	...
9	44.543087	19.342381	23.558	21.219	19.565	17.767	16.949	15.287	14.675	14.191	14.05	13.96	14.2	13.45	...
10	43.89241	19.230597	24.998	23.095	21.504	20.419	20.004	...	...	...	14.17	13.27	12.44	11.5	8.07
11	43.921101	19.240982	24.628	21.443	19.397	17.856	16.93	15.342	14.448	14.065	13.83	13.79	13.43	13.24	10.24
12	44.493095	19.435814	23.683	20.464	18.429	17.263	16.506	15.092	14.34	14.011	13.72	13.77	13.57	13.25	...
13	44.656075	19.535927	21.596	20.966	20.406	20.025	19.769	...	...	...	12.63	12.39	11.99	11.31	8
14	43.69643	19.301823	23.295	21.229	19.293	17.644	16.69	15.054	14.413	13.997	13.67	13.55	13.39	12.78	...
15	44.80117	19.622728	19.075	16.989	16.093	15.696	15.513	14.404	13.939	13.814	13.75	13.72	13.75	13.2	10.27
16	43.657982	19.346586	23.847	23.128	20.437	19.071	20.448	...	...	...	9.08	9.14	6.87	6.84	...
17	44.706165	19.618237	22.612	19.256	17.638	16.869	16.359	14.997	14.273	13.995	13.75	13.68	13.55	13.04	8.48
18	44.011776	19.457083	24.371	25.426	22.08	20.107	18.534	16.134	14.699	14.218	13.94	13.79	13.56	13.14	10.41
19	44.874004	19.721304	20.185	19.759	19.419	19.197	18.954	...	...	...	13.67	12.91	12.16	11.17	8.09
20	44.36845	19.627722	23.443	21.748	19.439	18.103	17.173	15.524	14.793	14.353	14.02	13.98	14.11	13.41	12.22
21	44.883926	19.784885	25.083	21.446	19.895	17.98	16.99	15.194	14.85	14.233	13.86	13.73	13.49	13.05	11.2
22	44.821747	19.790335	21.749	19.182	17.589	16.794	16.417	14.97	14.263	14.115	13.9	13.93	14.21	13.32	...
23	44.479301	19.713919	24.193	23.987	21.298	19.961	19.137	17.084	15.951	14.989	13.06	12.34	11.63	10.75	7.63
24	44.534443	19.749584	23.447	22.057	20.933	20.667	20.06	...	...	...	14.66	13.89	13.12	12.25	8.79
25	44.636703	19.830399	18.864	17.155	16.383	15.994	15.801	14.612	14.251	14.151	13.96	13.98	14.12	13.34	...
26	45.013542	19.973459	20.779	20.046	19.485	19.263	19.168	...	...	...	15.04	13.93	12.91	11.76	...
27	43.792133	19.640656	21.442	18.847	17.376	16.596	16.082	14.745	14.078	13.861	13.75	13.72	13.63	13.2	11.29
28	43.585831	19.61787	22.607	19.842	18.053	17.019	16.431	15.038	14.326	14.06	13.84	13.78	13.76	13.23	...
29	43.752075	19.738661	25.912	22.802	20.721	18.785	17.677	15.721	14.96	14.835	14.19	13.95	14.29	13.12	10.26
30	44.377293	19.956615	25.397	24.036	23.415	23.89	21.236	...	...	...	13.91	13.79	12.67	10.99	8.17
31	44.473091	19.986931	24.342	20.914	18.622	17.537	16.844	15.126	14.394	14.086	13.91	13.86	13.59	13.14	9.5
32	43.451626	19.729734	21.146	20.274	19.635	19.209	18.568	17.137	16.191	15.287	13.73	13.04	12.47	11.37	...
33	44.539505	20.08777	21.387	18.541	16.974	16.276	15.728	14.241	13.499	13.326	13.19	13.15	13.1	12.6	9.81

ID	α(2000)	δ(2000)	U	G	R	I	Z	J	H	K	3.6	4.5	5.8	8	24
34	43.477814	19.830866	22.544	21.019	20.219	19.844	19.413	...	...	...	14.32	13.54	12.81	11.72	...
35	44.154743	20.087011	22.441	20.785	19.064	17.664	16.852	15.348	14.718	14.477	13.93	13.84	12.33	12.03	7.72
36	44.022518	20.059565	22.808	22.05	20.941	20.413	20.115	...	...	...	14.49	13.79	13.59	11.88	7.99
37	43.863098	20.098879	20.749	18.189	16.863	16.227	15.85	14.551	13.93	13.749	13.74	13.73	13.92	13.22	...
38	44.52763	20.326477	24.81	23.525	22.099	21.318	20.57	...	...	...	13.14	12.09	11.12	10.05	6.48
39	44.037403	20.230776	23.267	21.082	18.723	17.537	16.955	15.101	14.169	13.956	13.68	13.64	13.36	13.13	...
40	43.309624	20.0951	21.532	18.633	17.103	16.456	16.039	14.771	14.008	13.848	13.62	13.6	13.57	12.97	...
41	44.530472	20.500483	22.718	21.206	19.696	18.83	18.217	15.953	14.985	14.035	12.51	11.83	11.11	10.35	7.24
42	43.348782	20.255596	24.657	23.226	22.164	21.679	20.67	...	...	...	14.71	13.65	12.77	11.53	...
43	43.489464	20.319742	23.635	22.913	21.533	20.754	20.165	...	...	...	14.68	13.84	12.78	11.82	7.71
44	43.582127	20.36952	23.14	21.071	18.812	17.748	17.164	15.551	14.544	14.356	14.01	13.95	13.55	13.33	11.85
45	44.790604	20.780897	19.556	17.5	16.478	16.033	15.764	14.636	14.134	13.925	13.86	13.85	14.39	13.26	...
46	43.631237	20.474005	24.881	21.166	19.046	17.647	16.82	15.254	14.438	14.162	13.73	13.67	13.43	13.09	9.78
47	43.975723	20.61377	23.24	21.384	19.287	17.85	17.06	15.418	14.669	14.439	14.05	13.99	13.96	13.18	...
48	43.53709	20.524986	22.72	19.288	17.58	16.809	16.314	14.899	14.188	13.979	13.87	13.79	13.76	13.03	10.43
49	44.144726	20.722004	22.304	19.555	17.839	17.067	16.688	15.11	14.39	14.307	13.93	13.94	13.64	13.19	10.07
50	44.679939	20.876045	24.363	20.912	18.842	17.669	16.994	15.428	14.638	14.247	14.08	13.97	13.6	13.14	...
51	44.679848	20.875883	24.363	20.912	18.842	17.669	16.994	15.428	14.638	14.247	14.07	13.98	13.59	13.23	...
52	43.795925	20.634935	24.01	21.881	19.942	18.104	17.053	15.4	14.777	14.449	13.96	13.91	14.08	13.27	11.44
53	44.599167	20.877443	22.244	20.924	20.248	19.887	19.394	...	...	...	14.48	13.61	12.73	11.8	...
54	44.873647	19.42891	19.22	18.5	17.959	17.538	17.183	...	...	...	13.66	12.95	12.16	11.16	7.59
55	44.568886	19.117891	...	...	...	...	...	...	...	...	13.45	13.15	12.3	12.19	10.24
56	44.600681	19.225142	...	...	...	...	...	...	...	...	12.96	12.66	11.93	11.87	8.66
57	43.699123	18.966953	...	...	...	...	...	15.554	14.906	14.178	...	13.45	13.06	11.75	...
58	44.597961	19.233231	...	...	...	...	...	...	...	...	13.03	12.94	11.98	12.08	9.39
59	44.820293	19.355543	...	...	...	...	...	16.024	15.187	14.387	13.32	13.02	12.57	9.62	7.13
60	44.942989	19.410385	...	...	...	...	...	15.964	15.389	14.78	13.95	13.8	13.5	13.01	10.87
61	43.626888	19.048973	...	...	...	...	...	...	...	...	14.11	13.99	14.19	12.1	...
62	43.81517	19.236662	...	...	...	...	...	...	...	...	9.71	9.78	9.32	7.43	5.81
63	44.789364	19.489986	...	...	...	...	...	...	...	...	13.91	13.86	13.55	12.98	10.45
64	44.006973	19.309507	...	...	...	...	...	16.406	15.52	15.192	13.32	13.19	11.91	9.69	7.14
65	44.657444	19.536034	...	...	...	...	...	13.719	12.972	12.757	12.42	12.26	11.88	11.4	8.11
66	44.707623	19.6173	...	...	...	...	...	...	...	...	14.18	13.93	13.27	12.47	8.34

ID	α(2000)	δ(2000)	U	G	R	I	Z	J	H	K	3.6	4.5	5.8	8	24
67	43.963638	19.439032	...	...	...	...	...	...	...	...	14.82	13.99	13.16	12.31	8.34
68	43.751339	19.488276	...	...	...	...	...	16.714	16.173	15.293	14.15	13.93	13.74	12.58	11.1
69	43.998035	19.600433	...	...	...	...	...	...	...	...	14.47	13.45	12.56	11.51	8.09
70	44.60133	19.822895	...	...	...	...	...	16.44	15.758	14.975	13.43	13.32	12.91	10.69	8.12
71	44.602158	19.824036	...	...	...	...	...	...	...	...	13.72	13.64	13.26	10.96	8.22
72	44.784702	19.985882	...	...	...	...	...	14.206	13.952	13.819	13.63	13.88	12.74	13.11	11.36
73	43.528725	19.673767	...	...	...	...	...	...	...	...	12.5	12.5	11.55	9.75	...
74	44.372917	19.951349	...	...	...	...	...	15.591	15.419	14.169	12.92	12.83	11.84	10.27	7.45
75	44.373798	19.952301	...	...	...	...	...	15.288	14.714	13.745	12.76	12.68	11.71	10.09	7.45
76	44.374474	19.953131	...	...	...	...	...	...	...	...	12.84	12.76	11.73	10.13	7.49
77	44.535118	20.011759	...	...	...	...	...	...	...	...	13.93	13.81	13.98	12.98	13.05
78	44.308788	20.003229	...	...	...	...	...	16.373	15.696	14.635	13.96	13.82	12.73	10.48	8.15
79	44.870068	20.167501	...	...	...	...	...	...	...	...	13.91	13.98	13.67	12.92	...
80	44.266129	20.012194	...	...	...	...	...	...	...	...	11.38	11.29	9.99	8.12	5.27
81	44.960476	20.314737	...	...	...	...	...	16.972	16.163	15.445	17.15	16.15	13.71	14.62	12.05
82	44.860107	20.338013	...	...	...	...	...	15.442	14.603	14.326	13.8	13.82	13.58	13.27	...
83	44.860565	20.338594	...	...	...	...	...	...	...	...	13.79	13.84	13.57	13.06	...
84	44.608593	20.333921	...	...	...	...	...	...	...	...	14.3	13.88	13.16	11.47	7.66
85	43.808071	20.134001	...	...	...	...	...	16.48	15.791	15.003	14.15	13.92	14.16	12.61	11.12
86	44.595943	20.378563	...	...	...	...	...	...	...	...	14.87	13.93	12.93	11.48	7.36
87	43.605026	20.141951	...	...	...	...	...	15.991	15.225	14.461	13.72	13.53	13.28	11.05	8.65
88	44.49007	20.414772	...	...	...	...	...	...	...	...	13.78	13.85	13.74	13.14	10.78
89	44.624302	20.463301	...	...	...	...	...	17.442	15.691	15.342	14.2	13.99	13.84	10.86	7.54
90	44.726746	20.498623	...	...	...	...	...	...	...	...	13.6	13.57	13.74	12.4	...
91	44.705269	20.595549	...	...	...	...	...	...	...	...	9.36	9.35	8.11	8.17	...
92	44.696575	20.5931	...	...	...	...	...	...	...	...	9.42	9.42	8.06	8.17	...
93	44.48312	20.487572	...	...	...	...	...	...	...	...	13.87	13.85	14.03	13.08	...
94	43.488861	20.228256	...	...	...	...	...	15.317	14.488	14.248	13.8	13.79	13.61	12.49	10.35
95	43.481182	20.229218	...	...	...	...	...	...	...	...	13.96	13.82	12.99	12.85	10.73
96	44.720802	20.58993	...	...	...	...	...	...	...	...	13.66	13.72	12.66	12.61	...
97	44.717953	20.5905	...	...	...	...	...	...	...	...	13.23	13.27	12.03	12.48	...
98	44.103378	20.419735	...	...	...	...	...	...	...	...	13.62	13.57	13.23	11.42	8.49
99	44.103985	20.421215	...	...	...	...	...	...	...	...	13.44	13.39	13.39	11.39	8.36

ID	α(2000)	δ(2000)	U	G	R	I	Z	J	H	K	3.6	4.5	5.8	8	24
100	44.69136	20.611719	...	...	...	...	...	...	...	...	13.93	13.75	11.89	13.05	...
101	44.136555	20.47328	...	...	...	...	...	...	...	...	13.07	13.03	12.63	11.4	9.35
102	44.135208	20.473461	...	...	...	...	...	...	...	...	13.13	13.09	12.78	11.45	9.69
103	44.135147	20.472649	...	...	...	...	...	...	...	...	13.14	13.11	12.79	11.51	9.59
104	43.258327	20.271177	...	...	...	...	...	16.087	15.268	14.826	13.39	13.28	12.01	9.84	...
105	43.428684	20.371786	...	...	...	...	...	14.458	13.864	13.558	13.32	13.26	13.18	12.72	11.65
106	43.575146	20.458281	...	...	...	...	...	17.099	16.052	15.438	14.32	13.98	14.18	12.12	9.01
107	43.363026	20.42993	...	...	...	...	...	...	...	...	12.69	12.51	12.27	10.92	...
108	43.568718	20.56469	...	...	...	...	...	...	...	...	10.53	10.23	9.09	9.07	6.06
109	43.577389	20.567202	...	...	...	...	...	...	...	...	10.22	10.61	8.78	9.23	5.86
110	43.570019	20.577526	...	...	...	...	...	...	...	...	12.91	12.92	10.72	10.42	9.35
111	44.061485	20.699289	...	...	...	...	...	17.055	16.018	15.186	14.25	13.89	13.78	13.12	9.65
112	43.779156	20.639679	...	...	...	...	...	...	...	...	13.94	13.92	13.46	13.05	...
113	44.709415	20.919003	...	...	...	...	...	...	...	...	13.89	13.84	13.39	13.32	...

[a] U, G, R, I, and Z are from SDSS database with entries in magnitudes and uncertainties in the 5-10% range.
[b] J, H, and K are from 2MASS database with entries in magnitudes and uncertainties in the 5-10% range.
[c] 3.6, 4.5, 5.8, 8.0, and 24 micron data are Spitzer data acquired for this work with entries in magnitudes and uncertainties in the 5-10% range.

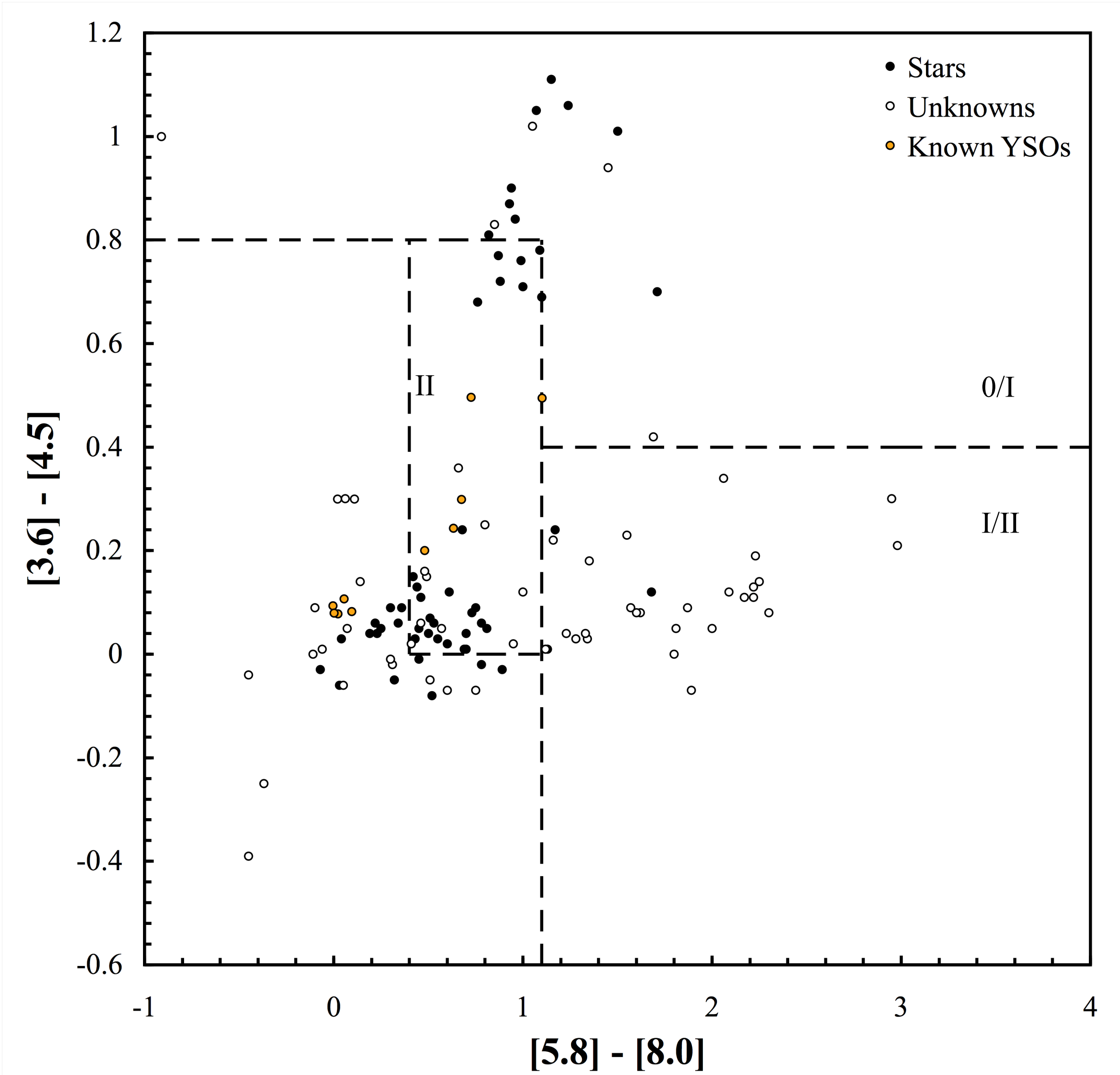

Figure 4-4. Color – color diagram of candidate 8 μm sample sources. Known YSOs are plotted for comparison. Magnitude uncertainties are in the 5-10% range.

defined by [5.8] – [8.0] colors greater than 1.1 and [3.6] – [4.5] colors less than 0.4 magnitudes. The Class 0/I region is defined [5.8] – [8.0] colors greater than 1.1 and [3.6] – [4.5] colors greater than 0.4 or for [5.8] – [8.0] colors < 1.1, [3.6] – [4.5] colors greater than 0.8. Class III YSOs and normal stars cannot be distinguished using these colors and occupy the same region. The second method originated in a search for protostars in the Elephant Trunk Nebula by Reach et al. (2004) and is outlined clearly by Rho et al. (2006) in a search for YSOs in the Trifid Nebula. It uses a combination of IRAC and MIPS magnitudes in order to attempt to better classify possible YSOs. This diagram is shown in Figure 4-5. This method defines two YSO regions corresponding to Class II sources and Class 0/I sources. The Class II region is defined by [8] – [24] colors between 2 and 5, and [3.6] – [5.8] colors between 0.0 and 1.35. The Class 0/I region is defined by [8] – [24] colors greater than 2.7 and [3.6] – [4.5] colors greater than 1.35. Again, Class III YSOs cannot be distinguished in this way, and together occupy the remaining portion of the plot.

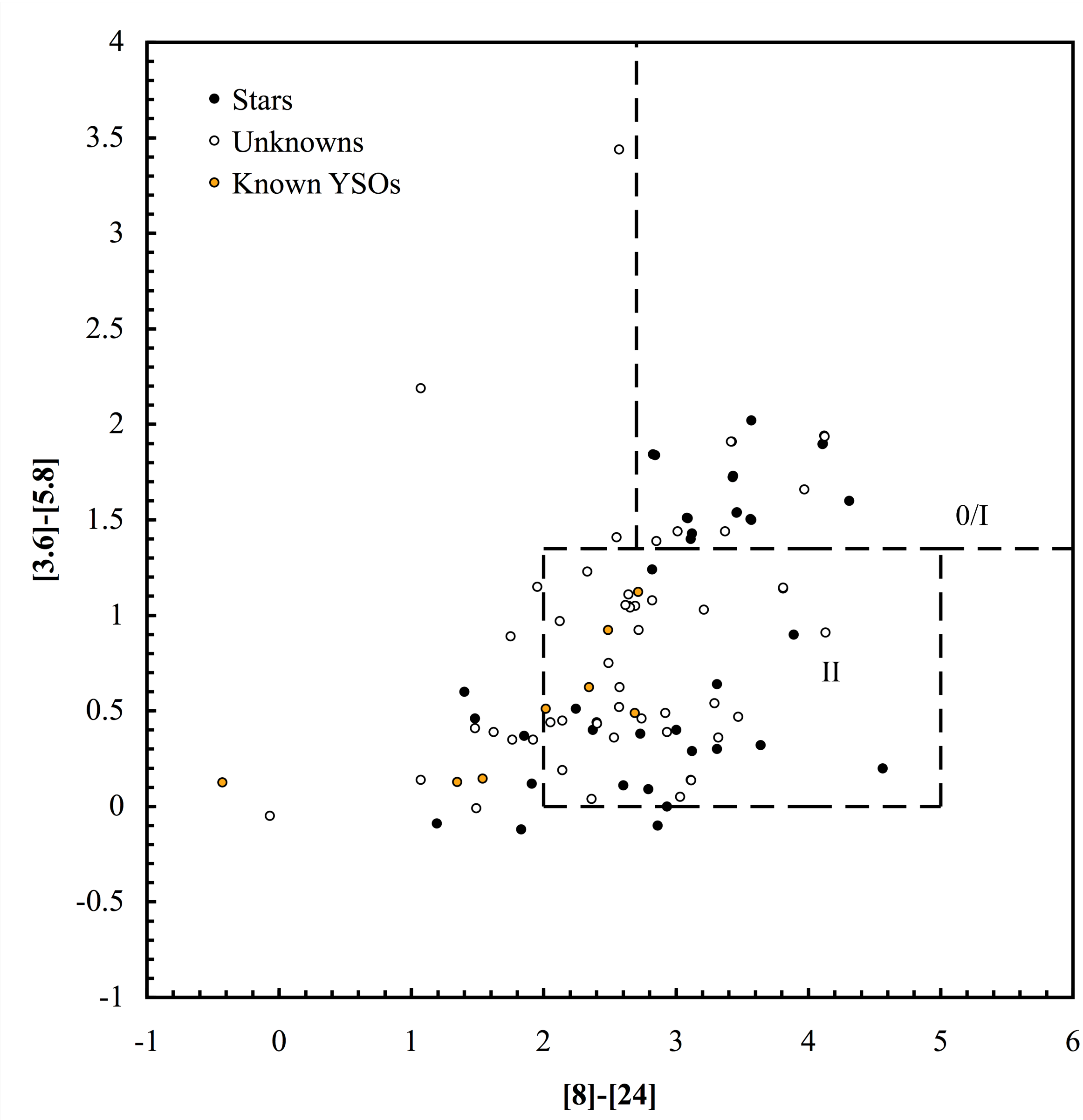

Figure 4-5. Color – color diagram of candidate 8 μm sample sources. The 8 known YSOs with 24 μm data are also plotted for comparison. Magnitude uncertainties are in the 5-10% range.

Chapter 5: Spectral Energy Distributions

5.1 The 70 μm Catalog; Discussion and SED's

Inspection of the 70 μm MIPS image resulted in a catalog of 23 sources in need of additional investigation. In order to further constrain the remaining unidentified candidates, spectral energy distributions (SEDs) were made to identify those sources with spectra typical of YSOs. SEDs can show distinct features that may enable their categorization into a specific class of YSO (Shu, Adams, & Lizano 1987). Class 0 objects are in the earliest stages of cloud collapse and their SEDs tend to peak beyond 100 μm. Class I sources are at a later stage of collapse but are still deeply embedded. Their SEDs show a large amount of infrared emission and peak near 100 μm. Class II YSOs are those with ongoing accretion and circumstellar disks. Their SEDs are characterized by excess infrared emission compared to that of a normal stellar photosphere. This emission peaks in the near infrared. Class III stars have SEDs that resemble normal stellar photospheres, making them difficult to distinguish based on SEDs alone. It has also been shown that a YSO's inclination can affect the structure of its SED (Whitney et al. 2003). Models of typical Class 0, I, and II SEDs are shown in figure 5-1.

A common way to determine YSO Class from SEDs is with a quantity called spectral index (α). The spectral index is defined by Lada (1987) by the relation:

$$\alpha = d \log (\lambda F_{\lambda}) / d \log (\lambda)$$

for a wavelength range of 2 to 25 μm. We obtain spectral indices of the 70 μm sample

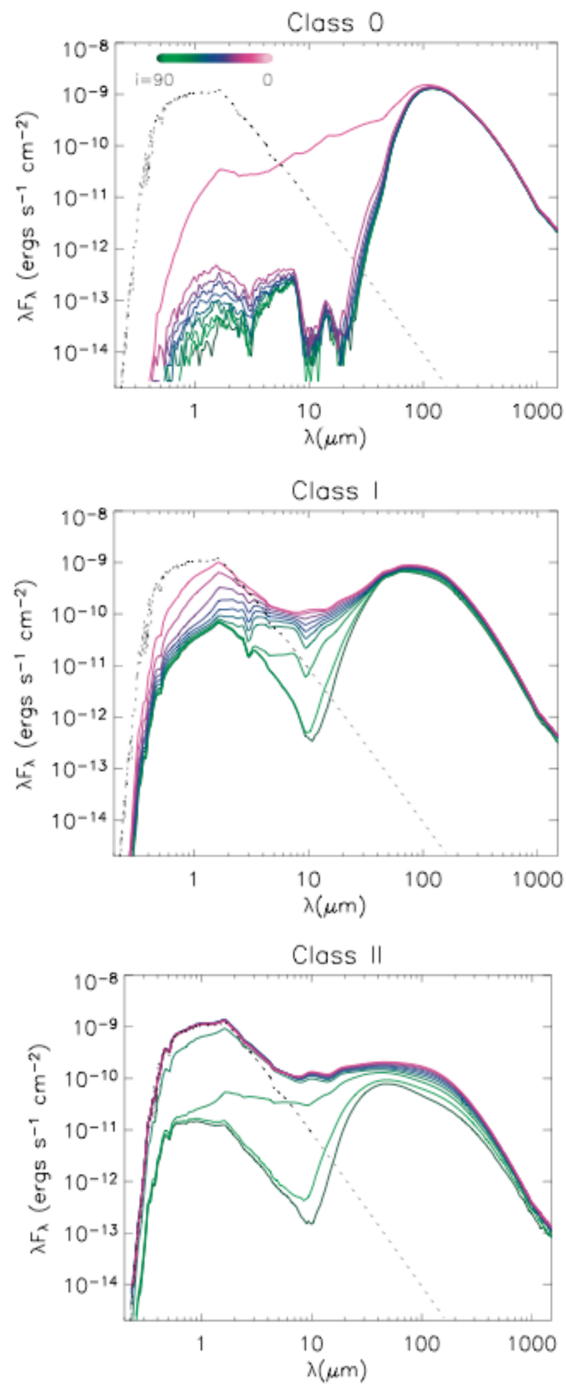

Figure 5-1. SED models of class 0, I, and II type YSOs. The colors indicate disk inclination; dark-green being edge-on and pink is pole-on. Figures were taken from Whitney et al. (2003). Dashed line indicates a normal stellar spectrum.

candidates by fitting a least-squares fit linear relationship from the 2MASS K (2.17 μm) band to the MIPS 24 μm band (when available). We use a revised classification scheme devised by Greene et al. (1994) to sort the candidates by this parameter. Sources with $\alpha > 0.3$ are considered Class 0/I. Those with $0.3 > \alpha \geq -0.3$ are classified as "flat spectrum" sources, while those with $-0.3 > \alpha \geq -1.6$ are considered Class II. Flat spectrum sources are thought to populate the transition region between Class I and Class II phases of stellar evolution. The sources with $\alpha < -1.6$ are classified as Class III YSOs. Harvey et al. (2006) note that the spectral index over an average of all spectral types is ~ -2.8.

While this classification system is very useful in sorting YSO candidates, background galaxy contamination can still be a major concern. While the SEDs of galaxies can vary greatly due to their type (E, Sab, Sbd, AGN, etc…) and evolutionary history, they do tend to have similar trends. In particular, their SEDs are likely to show increasing infrared emission with increasing wavelength. This emission is due to the illumination of interstellar dust by radiation from the general stellar population (Rowan-Robinson et al. 2005). By comparing the remaining 17 unidentified sources from the 70 μm sample to the sources known to be galaxies, we determined that the majority of the remaining sources were galaxies as well. Those candidates deemed to be galaxies (14) were eliminated from the candidate list. Through this method, nine possible YSO candidates have been found (numbers 4, 6, 46, 52, 54, 55, 57, 58, and 61 from Table 4-1). Using the classification criterion listed above, the spectral indices and possible YSO classes of these objects are given in table 5-1 along with known YSOs found by this method. SEDs are shown in Figure 5-2, except for the stars HD18066 and TYC 1227-297-1, which were bright enough to saturate the images and therefore do not have measured fluxes. SEDs of the known YSOs detected using this method are also shown in Figure 5-2 for comparison.

Table 5-1

70 μm Sample YSO Candidates and Known YSOs

ID	α(2000)	δ(2000)	Spectral Index (α)	YSO Class
E 02553+2018	02 58 11.23	20 30 03.5	-0.9521	II
4	02 58 06.41	20 19 32.8	0.236	"flat"
6	02 57 19.19	20 30 10.3	-3.2404	III
Lkhα 264	02 56 37.56	20 05 37.1	-0.395	II
Lkhα 262	02 56 07.99	20 03 24.3	-0.7622	II
Lkhα 263	02 56 08.42	20 03 38.6	-1.139	II
RX J0258.3+1947	02 58 16.09	19 47 19.6	-1.1621	II
46	02 59 29.73	19 25 44.5	0.0146	"flat"
52	02 54 45.20	20 17 12.6	-2.6872	III
54	02 57 01.15	20 05 40.3	-2.6831	III
55	02 57 55.01	19 42 50.2	-0.1327	"flat"
57	02 59 45.27	19 18 51.2	-2.5442	III
58	02 57 50.66	19 48 02.2	-1.6417	III
61	02 54 37.54	19 59 22.3	-1.9097	III

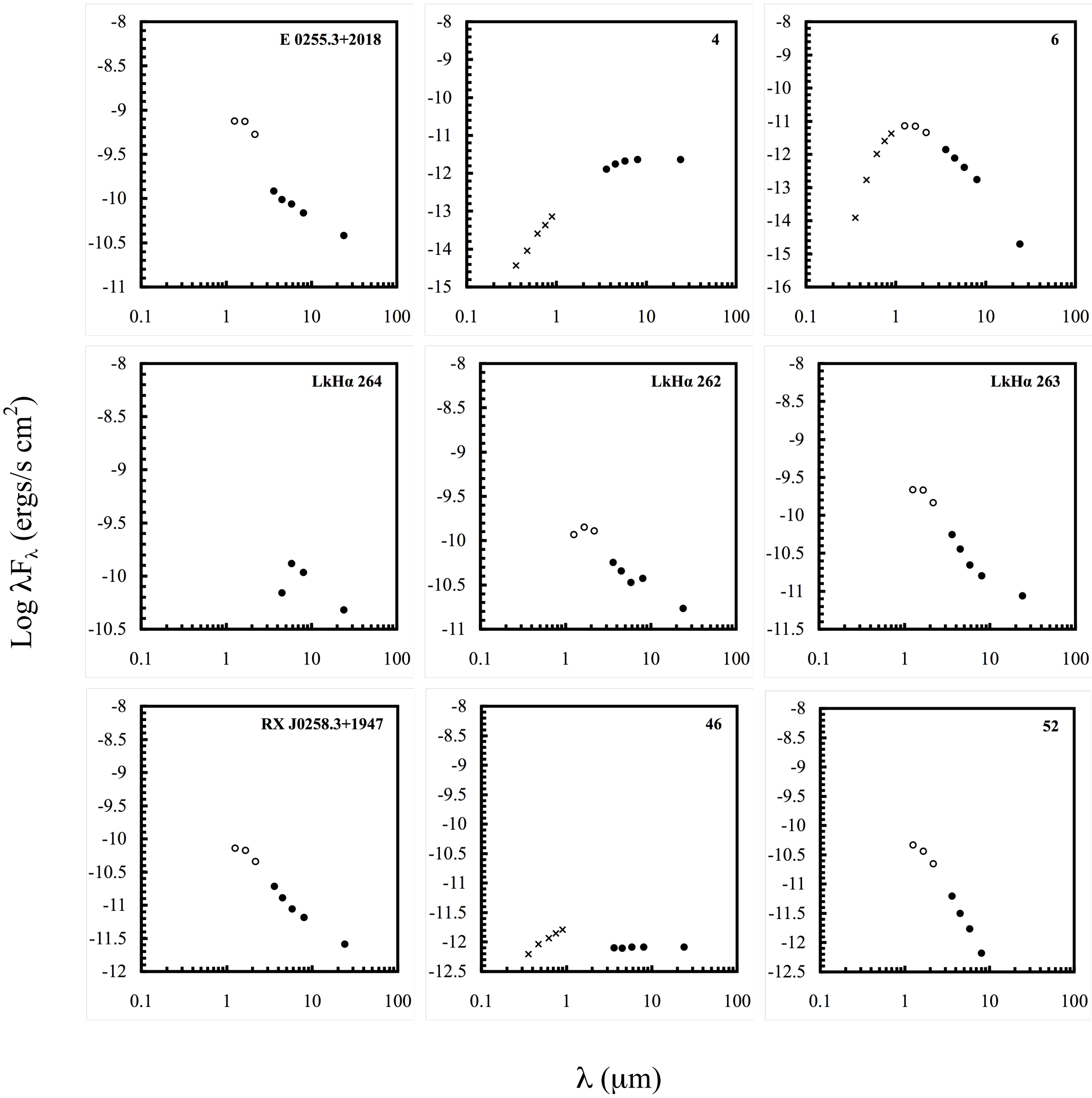

Figure 5-2. SEDs of observed MBM 12 objects from 70 μm sample. IRAC (3.6, 4.5, 5.8, and 8.0 μm) and MIPS (24 μm) fluxes (filled circles) are combined with data from 2MASS (open circles) and SDSS (crosses). SEDs are labeled with either their known name or the identification number designated in Table 4-1.

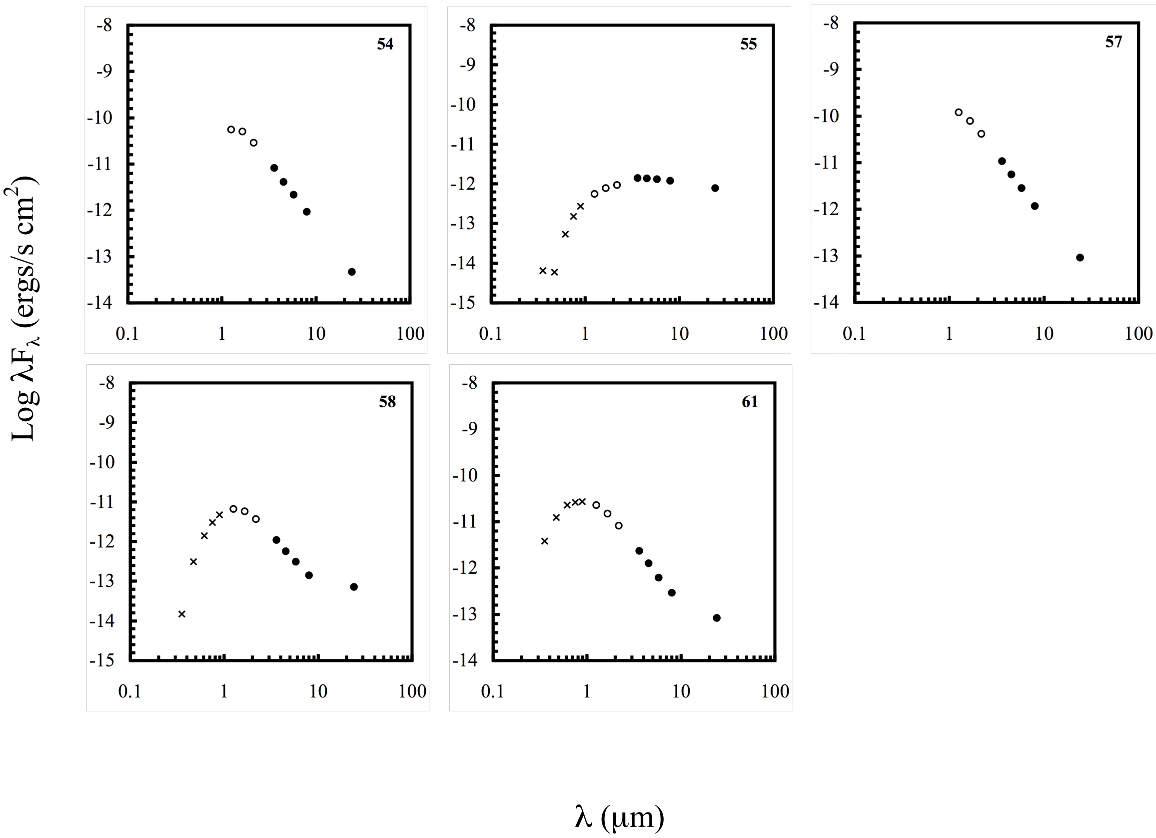

Figure 5-2. continued.

Because the index of an average star is within the range of our Class III spectral index classification, we are not able to distinguish those within this range from background stars. The positions of all objects in Table 5-1 are illustrated in Figure 5-3.

5.2 The 8 μm Catalog; Discussion and SEDs

In Section 4.1, by using a color – magnitude diagram scheme devised by Harvey et al. (2006), we compiled a list of 113 strong candidate sources from the 8 μm sample. Eleven of these sources were eliminated either due to being duplicate detections or erroneous due to saturated pixels. Fifty of the remaining sources are known to be stars from their corresponding Sloan data. While the combination of these methods is capable of eliminating background galaxies from the candidate list, the 52 unidentified sources still require further analysis to rule out the possibility of being extragalactic. Using visual inspection in the same manner as for the 70 μm sample, those sources with SEDs typical of galaxies were removed from the candidate list. In all, 25 sources were removed by this method. Eleven other sources, by only having detections at a few wavelengths, did not have enough data points to be distinguishable as either a star or a galaxy. To ensure the strongest possible candidate list, these were also eliminated. This results in a list of 66 possible YSO candidates.

With these remaining candidates, we identify their potential YSO type by 3 different methods. By combining methods we hope to find the most probable class (if the source is indeed a YSO) and see how well the various methods correlate with each other. We categorize this list of YSO candidates via the spectral index and two color – color classification schemes. As for

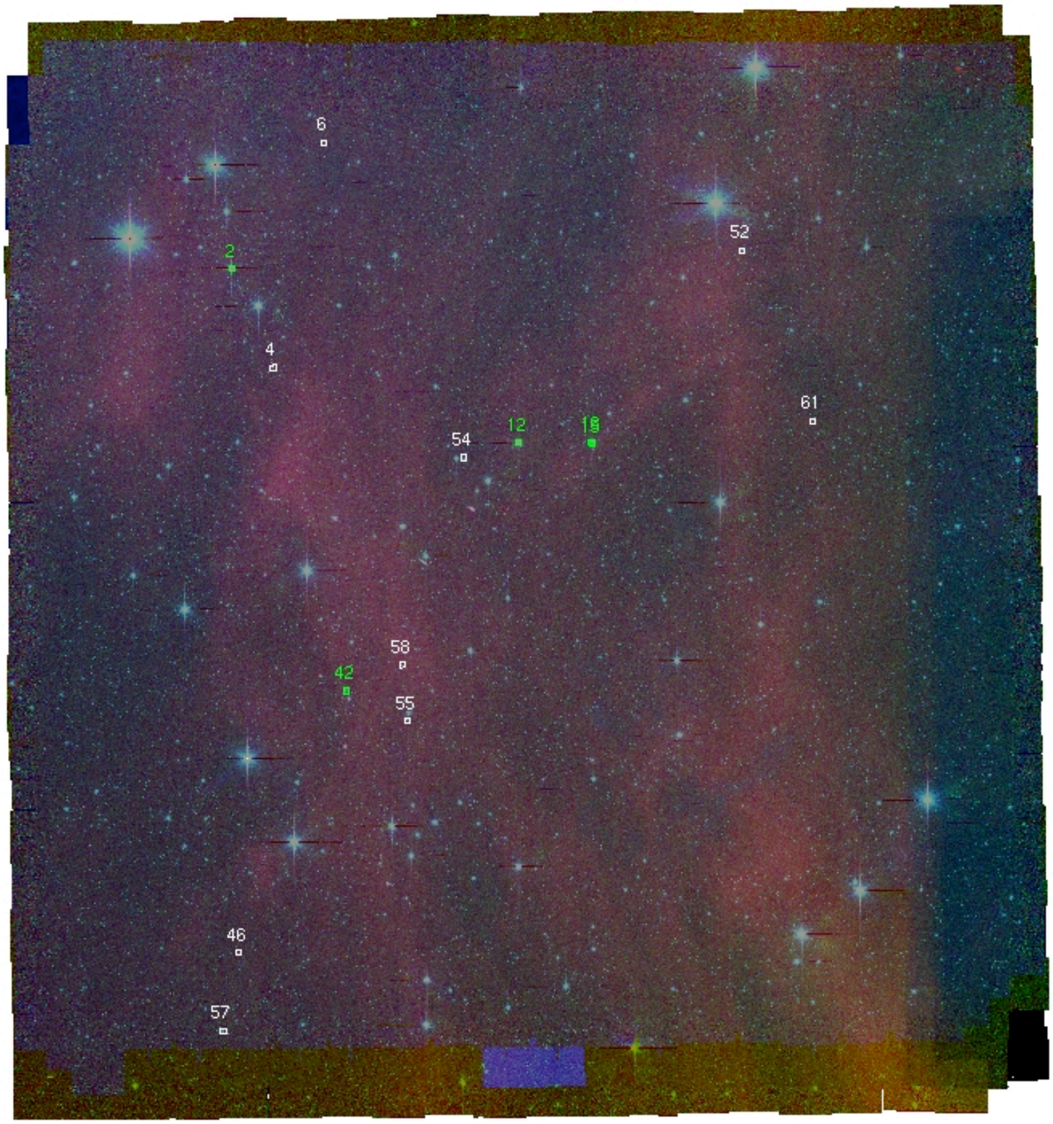

Figure 5-3. Positions of YSO candidates (white) from the 70 μm sample along with five known YSOs (green) from Luhman (2001). All are labeled with their number designations according to Table 4-1. Because of the extremely close proximity of LkHα 262 to LkHα 263 (15 and 16), they appear as only one box.

the 70 μm sample, we use the spectral index classification format by Greene et al. (1994), with $\alpha > 0.3$ being Class 0/I, $0.3 > \alpha \geq -0.3$ corresponding to a "flat spectrum", $-0.3 > \alpha \geq -1.6$ being Class II, and $\alpha < -1.6$ representing Class III YSOs. Using these definitions, 4 candidates are classified as Class 0/I (6.06%), 16 as "flat" (24.24%), 21 as Class II (31.81%), and 25 as Class III (37.88%). The color – color methods used are those of Allen et al. (2004) and Rho et al. (2006). The classifications of each method are described in Table 5-2. The categorization of all sources using each process is displayed in Table 5-3 with ID numbers from Table 4-4. Fifty sources fell into one of the regimes described by Allen et al. (2004) and 32 into those of Rho et al. (2006). Many of the classifications shown in Table 5-3 are in good agreement with each other. If we consider the sources described by their spectral index as "flat" as either Class I or II sources, 36 (72%) of the designations from the Allen classification and 30 (93.75%) from the Rho classification agree completely or partially with the categorization from the spectral index. Examples of partial agreements are I/II with II or 0/I with "flat". The two sources that did not agree from the Rho classification have spectral indices very close to the limits proposed by Greene et al. (1994) (-1.601 for source number 6 and -0.313 for source number 41). Twenty-six of the sources were categorized by both the Allen and Rho methods, and of these, 20 (76.92%) agreed with each other. Of these 20, all agree with the designations according to their spectral index. The SEDs of the 66 candidates are shown in Figure 5-4 and their positions are presented in Figure 5-5.

For comparison purposes, the spectral indices of the acknowledged YSO members of MBM 12 were calculated. The spectral indices of the known YSOs in MBM 12 reveal that, of the ten we detected, five are classified as Class II YSOs, with the others being Class III. This is

Table 5-2

Classification Criteria

Color	Class 0/1	Class I/II	Class II
[3.6] – [4.5]	≥ 0.4	< 0.4	0 to 0.8
[5.8] – [8.0]	≥ 1.1	> 1.1	0.4 to 1.1
[3.6] – [5.8]	> 1.35		0 to 1.35
[8.0] – [24]	> 2.7		2 to 5

Table 5-3

Spectral Index and YSO Class

ID	Spectral Index (α)	Class[a]	Class[b]	Class[c]
1	-2.075	III	…	…
2	-0.004	"flat"	0/I	…
3	-2.463	III	…	…
4	0.027	"flat"	0/I	0/I
5	-2.442	III	II	…
6	-1.601	III	…	II
7	0.015	"flat"	II	0/I
8	-2.170	III	…	…
9	-2.405	III	II	…
10	-0.016	"flat"	0/I	0/I
11	-1.398	II	…	II
12	-2.303	III	…	…
13	-0.613	II	II	II
14	-2.003	III	II	…
15	-1.489	II	II	II
17	-0.739	II	II	II
18	-1.399	II	II	II
19	-0.244	"flat"	II	0/I
20	-2.060	III	II	…
21	-1.707	III	II	…
22	-2.412	III	…	…
23	-0.133	"flat"	II	0/I
24	-0.106	"flat"	II	0/I
25	-2.366	III	…	…
26	0.914	0/I	0/I	…
27	-1.870	III	II	…
28	-2.287	III	II	…
29	-1.129	II	I/II	…
31	-1.083	II	II	II
32	-0.078	"flat"	0/I/II	…
33	-1.506	II	II	II
34	0.128	"flat"	II	…
35	-0.195	"flat"	…	0/I
36	0.292	"flat"	0/I	II
37	-2.548	III	II	…
38	0.236	"flat"	0/I	0/I
39	-2.221	III	…	…
40	-2.268	III	II	…
41	-0.313	II	II	0/I
42	0.772	0/I	0/I	…

43	0.432	0/I	0/I	0/I
44	-1.914	III	…	…
45	-2.558	III	I/II	…
46	-1.203	II	…	II
47	-2.024	III	II	…
48	-1.471	II	II	II
49	-1.239	II	…	II
50	-2.029	III	II	…
52	-1.734	III	II	…
53	0.244	“flat”	0/I	…
57	-1.226	II	I/II	…
60	-1.412	II	II	II
63	-1.167	II	II	II
66	-0.004	“flat”	II	II
67	0.188	“flat”	0/I	0/I
68	-1.290	II	I/II	…
69	0.102	“flat”	0/I	0/I
72	-1.906	III	…	…
82	-2.093	III	…	…
85	-1.379	II	I/II	…
86	0.711	0/I	0/I	0/I
88	-1.366	II	…	II
94	-1.330	II	I/II	II
101	-1.003	II	I/II	II
105	-2.139	III	II	…
111	-0.796	II	II	II

[a]From spectral index.
[b]From Allen et al. (2004) color – color criterion.
[c]From Rho et al. (2006) color – color criterion.

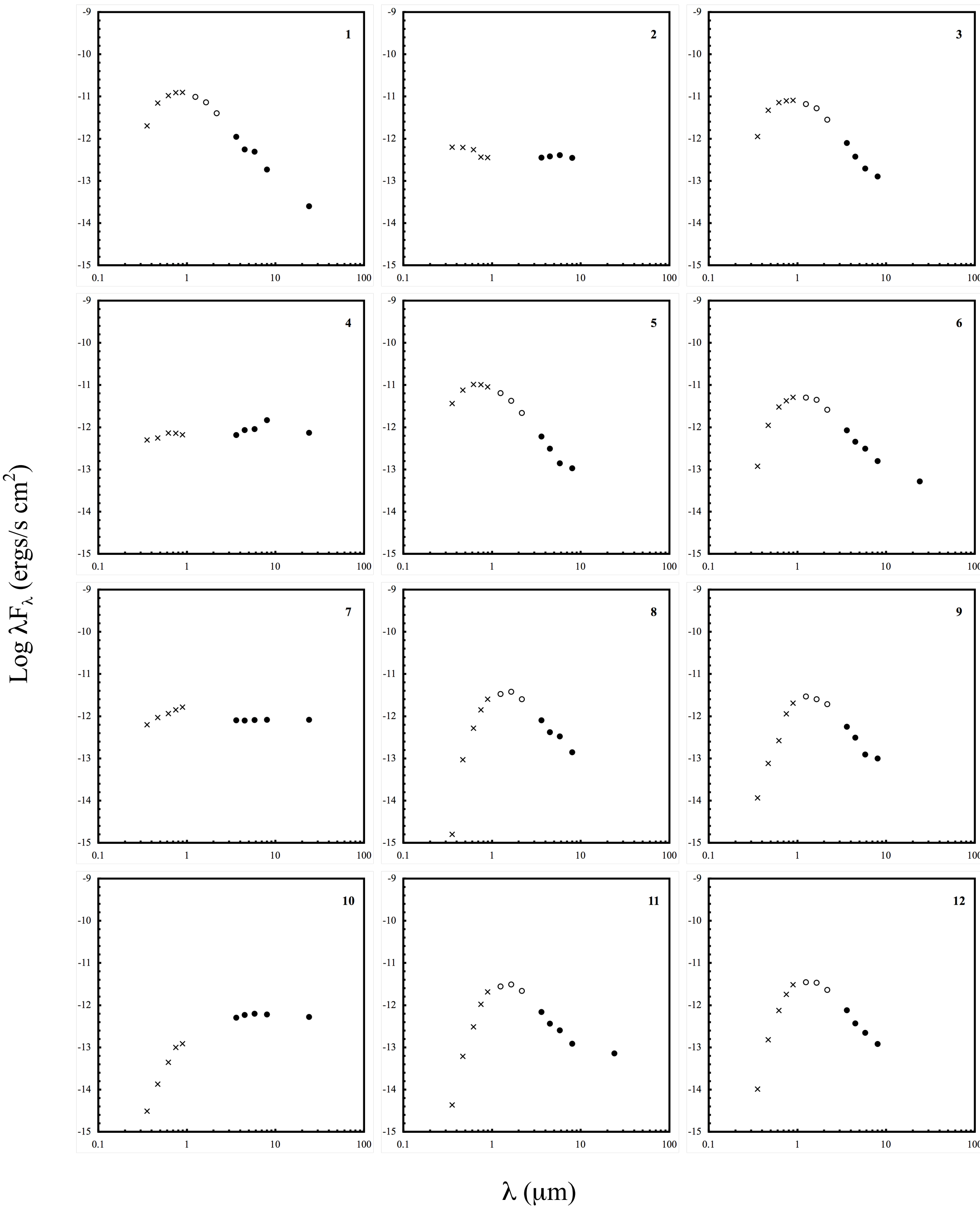

Figure 5-4. SED of candidates from 8 μm sample. IRAC and MIPS, 2MASS, and SDSS data are filled circles, open circles, and crosses respectively. Labels are from ID number given in Table 4-4.

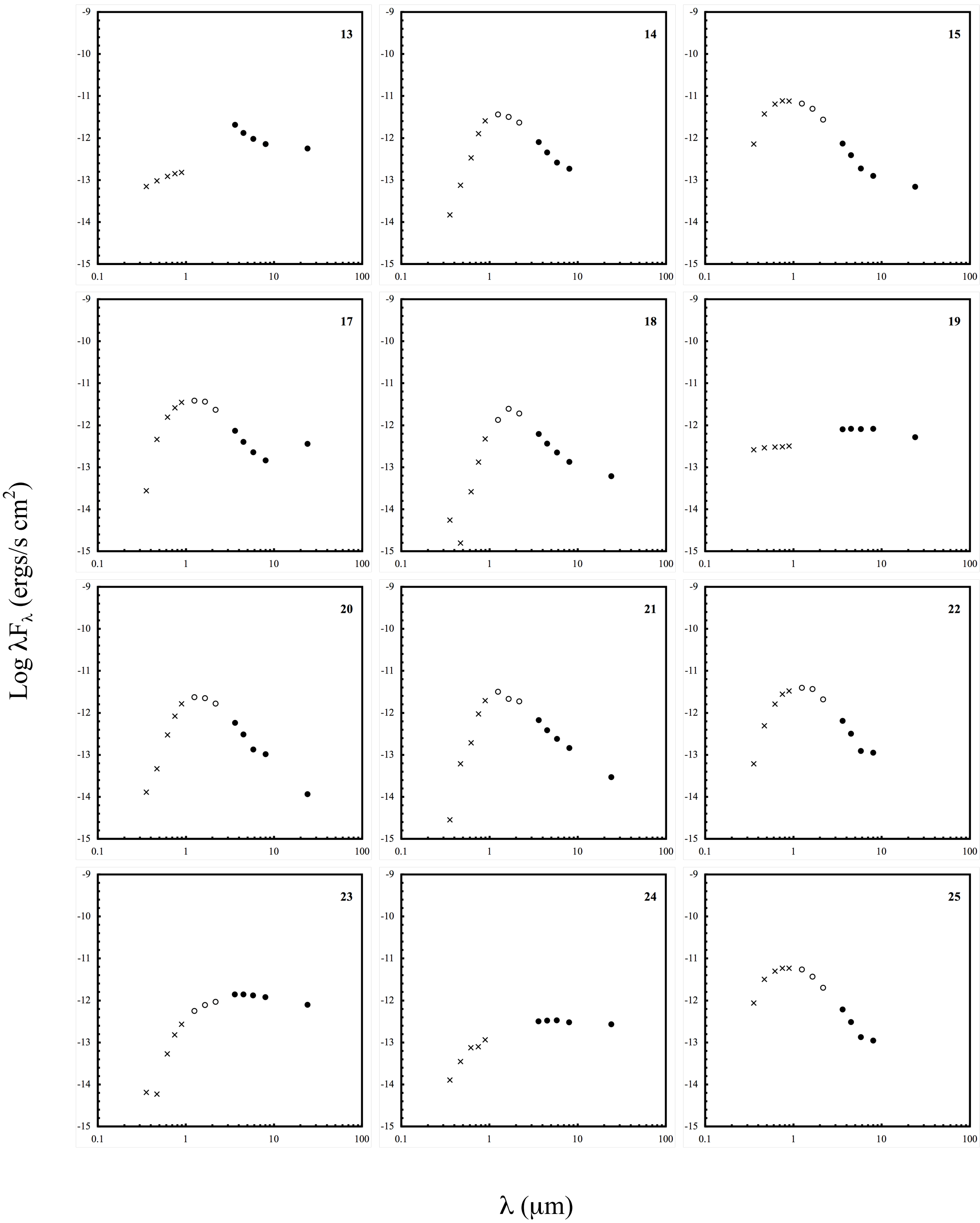

Figure 5-4 continued.

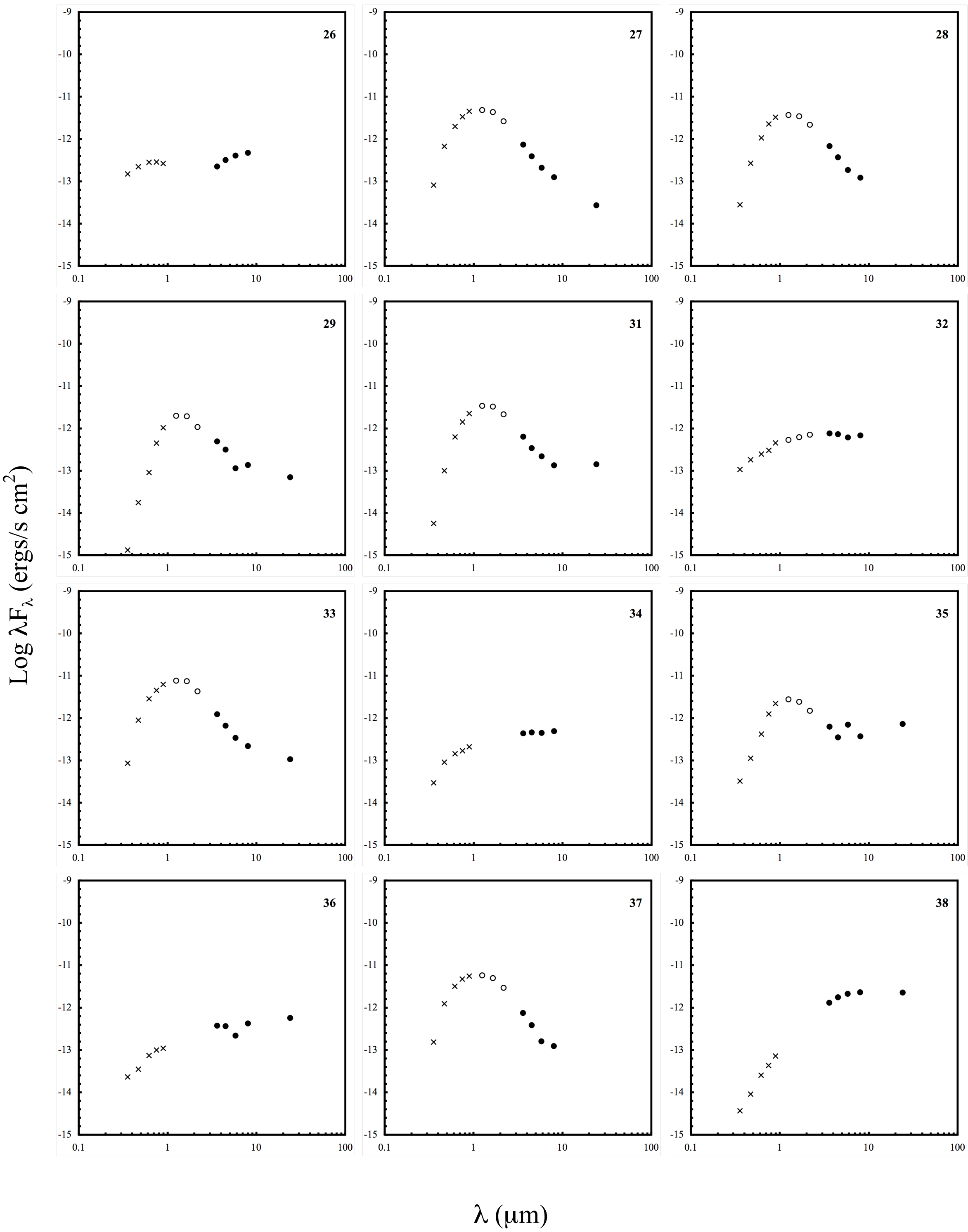

Figure 5-4 continued.

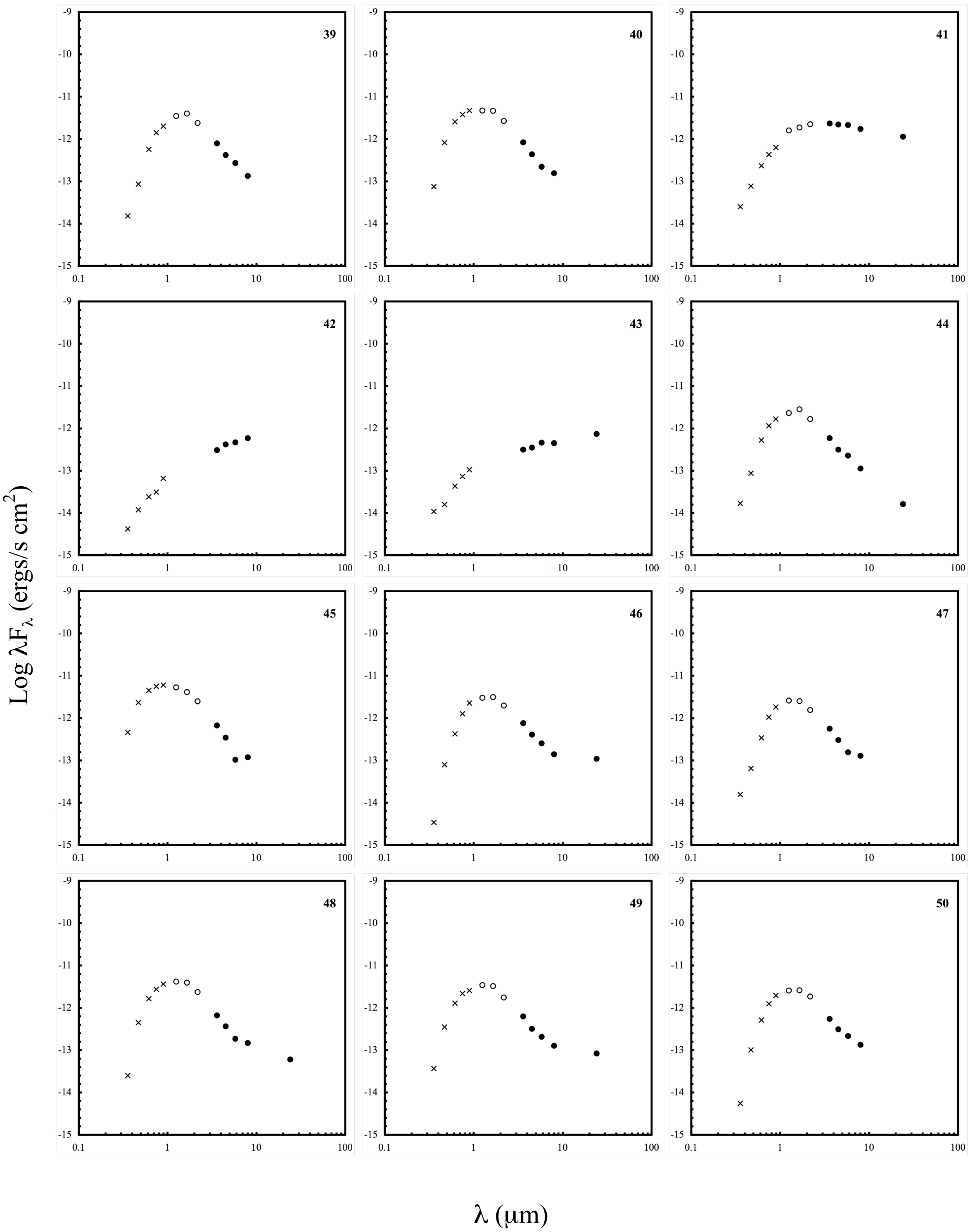

Figure 5-4 continued.

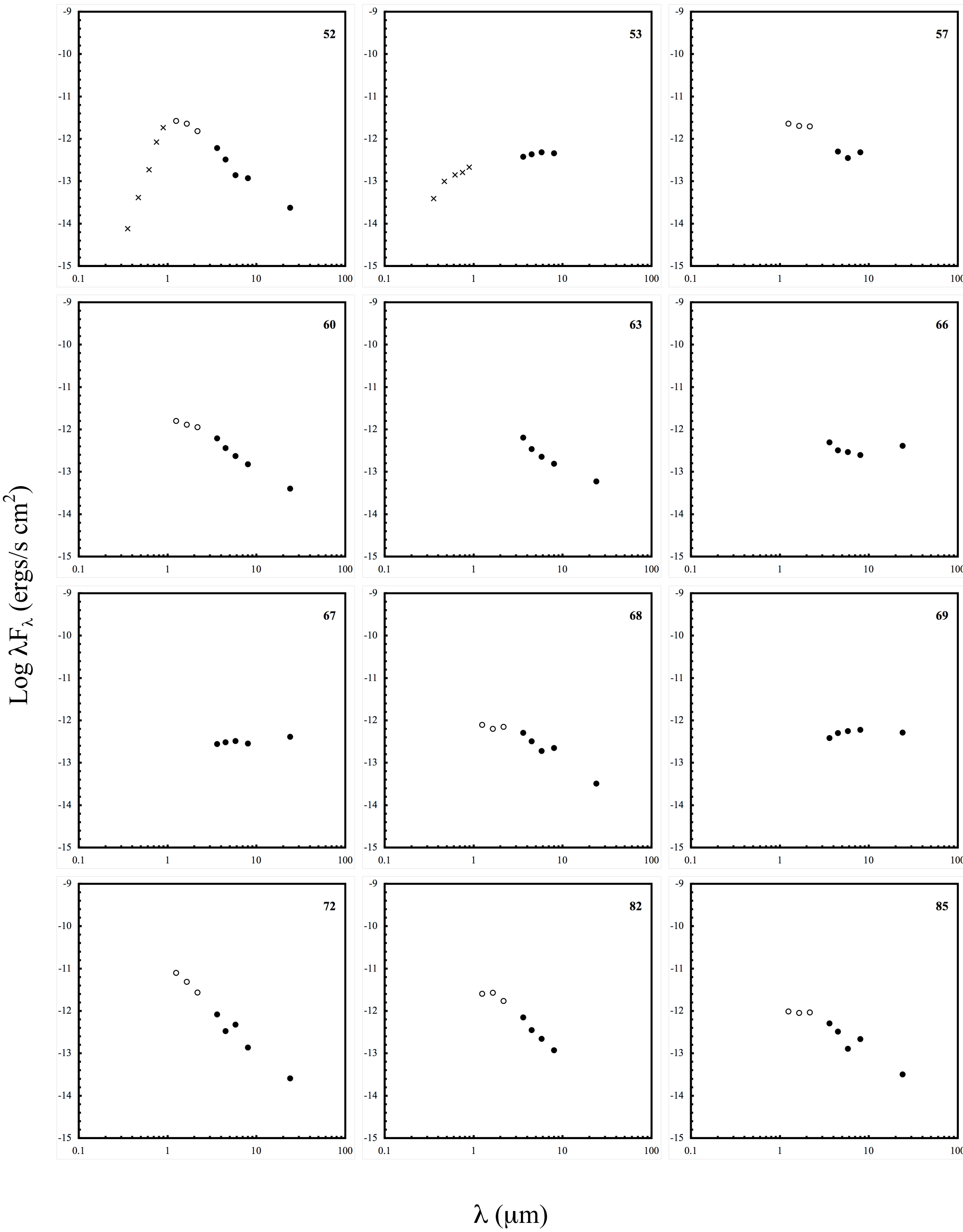

Figure 5-4 continued.

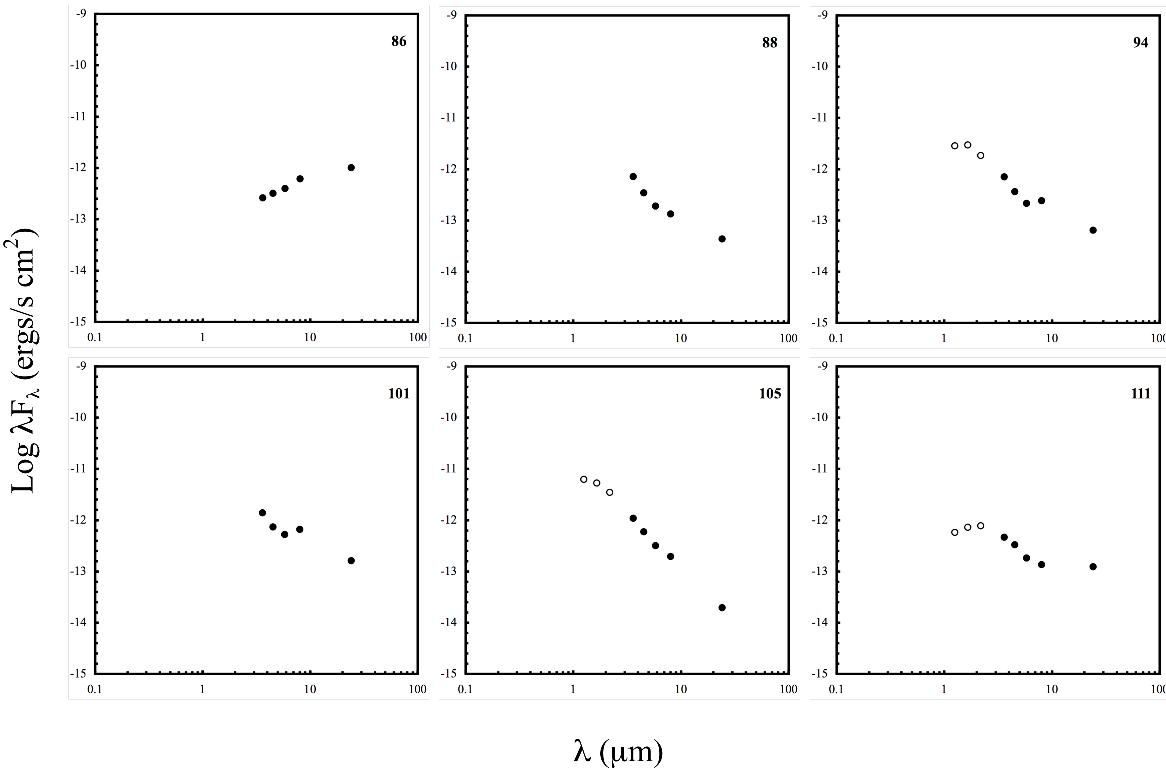

Figure 5-4 continued.

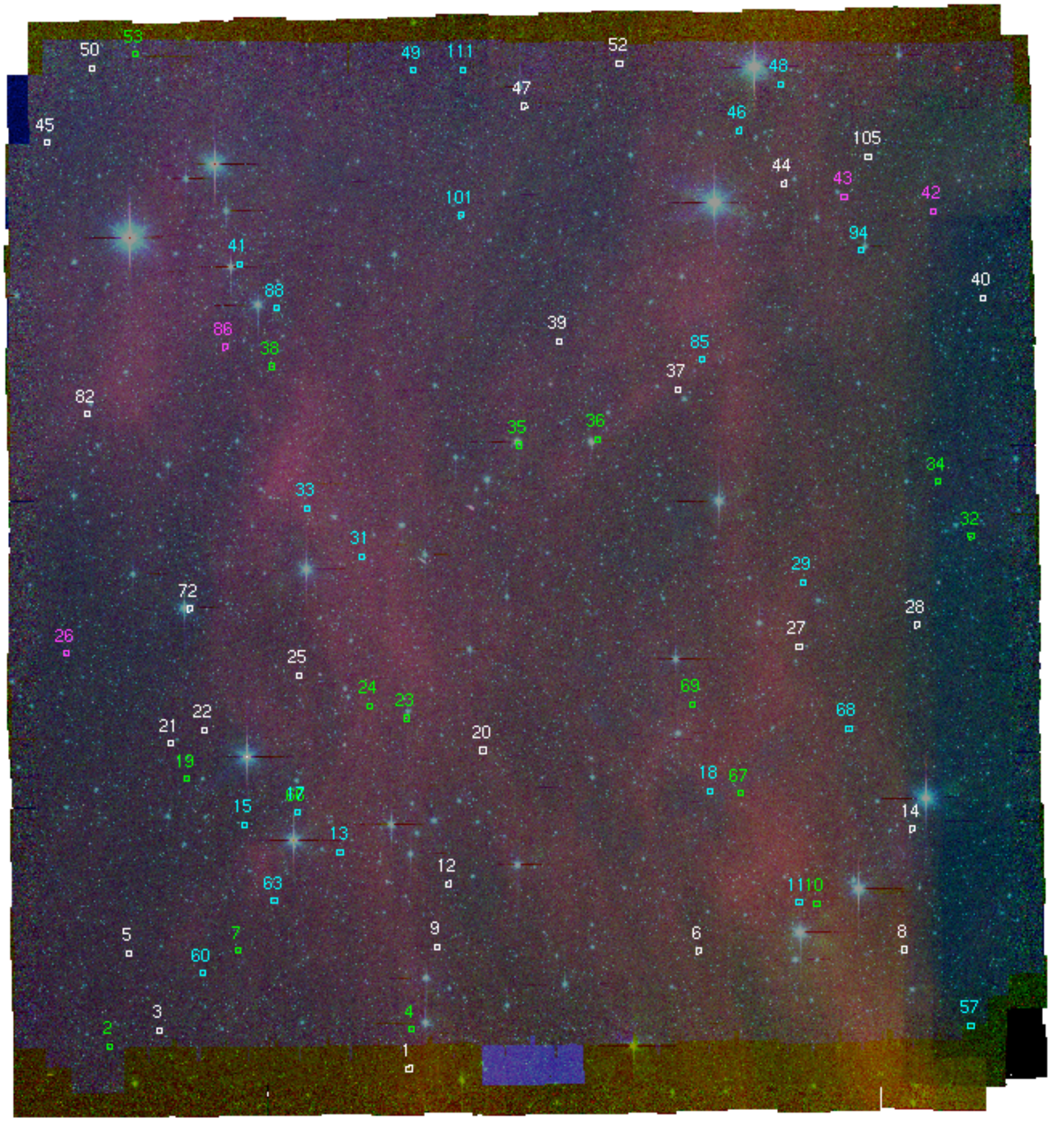

Figure 5-5. YSO candidates originating from 8 μm sample. Colors are based on spectral indices: Class 0/I (magenta), "Flat" (green), Class II (light blue), and Class III (white).

consistent with Figure 4-3, which shows half of the known YSOs are indistinguishable from normal stars. Figure 5-6 shows the spectral indices of known YSOs plotted with new candidate members. This diagram makes clear where the most likely Classes of our candidate YSOs lie. It also shows the depth of our search compared to the magnitudes of those YSOs already known. It is our hope that this depth will lead to the unveiling of YSOs previously undetected.

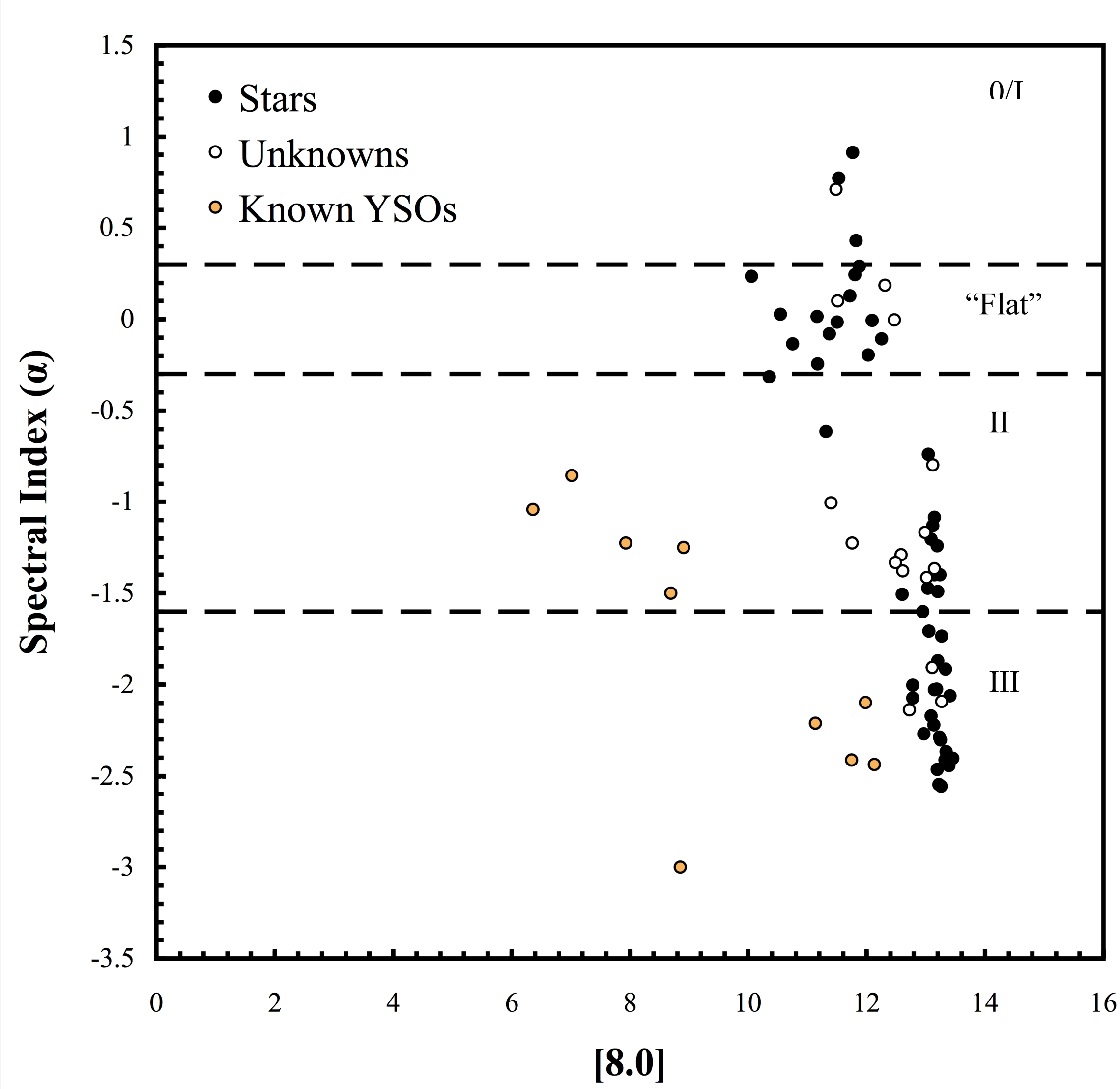

Figure 5-6. Spectral index vs. 8 μm magnitude. Dashed lines indicate spectral index limits from Greene et al. (1994). Note how much fainter the Spitzer data YSO candidates are compared to the magnitudes of the known YSOs.

Chapter 6: Results and Conclusion

6.1 Summary of Results

MBM 12 is a high-latitude molecular cloud that has visual extinction properties on the boundary between darkness and translucency. It is a productive star-forming region with 12 already known members. We have presented new Spitzer images of MBM 12 in an attempt to identify new candidate young stellar objects. In order to meet this end, we have taken several complementary approaches.

First, a visual inspection of the 70 μm MIPS image for point sources with strong infrared excess was performed to identify potential deeply embedded sources. This resulted in a list of 14 objects, five of them being previously known T Tauri stars. The remaining 9 sources were then investigated using their Spectral Energy Distributions (SEDs), and more specifically, the slope of their SED, called the spectral index. Six sources were identified as having spectral indices typical of Class III YSOs and 3 showed spectral indices in the limit of "flat" YSOs. Since Class III objects are hard to distinguish from background stars, we removed these from our list of best possible YSO candidates. This results in a list of 3 high-quality YSO candidates from the 70 μm data.

We then produced a second candidate list, this time using the 8 μm IRAC image as the basis for our source catalog. Then, with the combination of color – magnitude and color – color classification schemes, we procured a list of 66 possible YSO candidates. By next analyzing their SEDs and calculating spectral indices, we found out which class the YSO candidates were most likely to belong to. We used the combination of spectral index and color – color classification methods already proven in other star-formation regions to reveal the best YSO candidates. The colors of ten of the 66 candidates did not fit into the class boundaries of either color – color diagram. All of these are designated as Class III objects by their spectral indices. Since Class III sources can be difficult to distinguish from normal stars; these are removed from our list of the best candidates. These we consider lower priority candidates and are tabulated in Table 5-3. There are 30 sources that meet one color – color classification method requirement, but not the other. These we consider 'good' candidates. The best candidates are those that satisfy both color – color classification criteria. There are 26 sources that fit these conditions. The three sources found by visual inspection in the 70 μm sample to be good YSO candidates were also found to be good candidates using this method (ID #'s 7, 23, and 38 from Table 4-4 and 46, 55, and 4 from Table 4-1, respectively). All three have "flat" spectral indices. These three sources, along with 23 others that meet all color – color and color – magnitude requirements that are not categorized as Class III by their spectral index we consider 'excellent' YSO candidates. Two are considered Class 0/I by their spectral index (#'s 43 and 86 from Table 4-4). Eleven are deemed as "flat" according to their spectral index (#'s 4, 7, 10, 19, 23, 24, 36, 38, 66, 67, and 69 from Table 4-4). The last thirteen are identified by their spectral index as Class II (#'s 13, 15, 17, 18, 31, 33, 41, 48, 60, 63, 94, 101, and 111 from Table 4-4). A summary of our best, and, thus, highest priority YSO candidates is presented in Table 6-1 with their visual magnitudes (if available) from SDSS data and probable YSO Class.

Table 6-1

Final Catalog of the Best YSO Candidates

ID	α(2000)	δ(2000)	G[a]	R[b]	YSO Class
4	44.625526	19.22522	19.061	18.458	“flat”
7	44.873646	19.428909	18.5	17.959	“flat”
10	43.89241	19.230597	23.095	21.504	“flat”
13	44.656075	19.535927	20.966	20.406	II
15	44.80117	19.622728	16.989	16.093	II
17	44.706165	19.618237	19.256	17.638	II
18	44.011776	19.457083	25.426	22.08	II
19	44.874004	19.721304	19.759	19.419	“flat”
23	44.479301	19.713919	23.987	21.298	“flat”
24	44.534443	19.749584	22.057	20.933	“flat”
31	44.473091	19.986931	20.914	18.622	II
33	44.539505	20.08777	18.541	16.974	II
36	44.022518	20.059565	22.05	20.941	“flat”
38	44.52763	20.326477	23.525	22.099	“flat”
41	44.530472	20.500483	21.206	19.696	II
43	43.489464	20.319742	22.913	21.533	0/I
48	43.53709	20.524986	19.288	17.58	II
60	44.942989	19.410385	…	…	II
63	44.789364	19.489986	…	…	II
66	44.707623	19.6173	…	…	“flat”
67	43.963638	19.439032	…	…	“flat”
69	43.998035	19.600433	…	…	“flat”
86	44.595943	20.378563	…	…	0/I
94	43.488861	20.228256	…	…	II
101	44.136555	20.47328	…	…	II
111	44.061485	20.699289	…	…	II

[a]Magnitude from SDSS in G band (centered on 4686 Å)
[b]Magnitude from SDSS in R band (centered on 6165 Å)

6.2 Discussion

The best YSO candidates above are shown in Figure 6-1 superimposed on the three-color IRAC image of our region. Figure 6-2 shows the best candidates on the image, but now including the CO(1-0) contours of MBM 12. It is clear from this figure than only 10 of the 26 best candidates are projected within the CO boundary of the cloud. Thus, if a new wave of star formation is occurring in the cloud, it would almost certainly comprise only these objects. The 11 already-known T Tauri stars that are within our image boundary are all projected within the CO contours of the cloud and so it is likely that a younger YSO population would be even more clustered in the denser CO regions. The lack of such noticeable for our best YSO candidates indicates that, if there is a newer wave of star formation in MBM 12, it is likely to comprise only a few stars and not the dozen or so that formed earlier.

An older generation of newly formed stars would be $\sim 10^8$ years old and would have moved away from the cloud (Briceño et al. 1997). Some of our best YSO candidates that leaked away from the CO boundaries could indeed be members of an older population of star formation. The other objects, outside the CO boundary are either: 1) regular stars or galaxies, 2) YSOs that have formed in previous era of star formation older than that of the 11 known objects in the T – association (because they have had time to migrate away from the parental cloud), or 3) they are field dwarf stars that have no connection with MBM 12 (Briceño et al. 1997). Possibility would only pertain to those sources classified as Class II or older. Possibilities 1) and 3) are most likely, though the only way to be sure is to examine each object spectroscopically. Given the relatively small number of known YSOs, it is unlikely that this quantity of sources could be from an older generation of objects formed from the cloud.

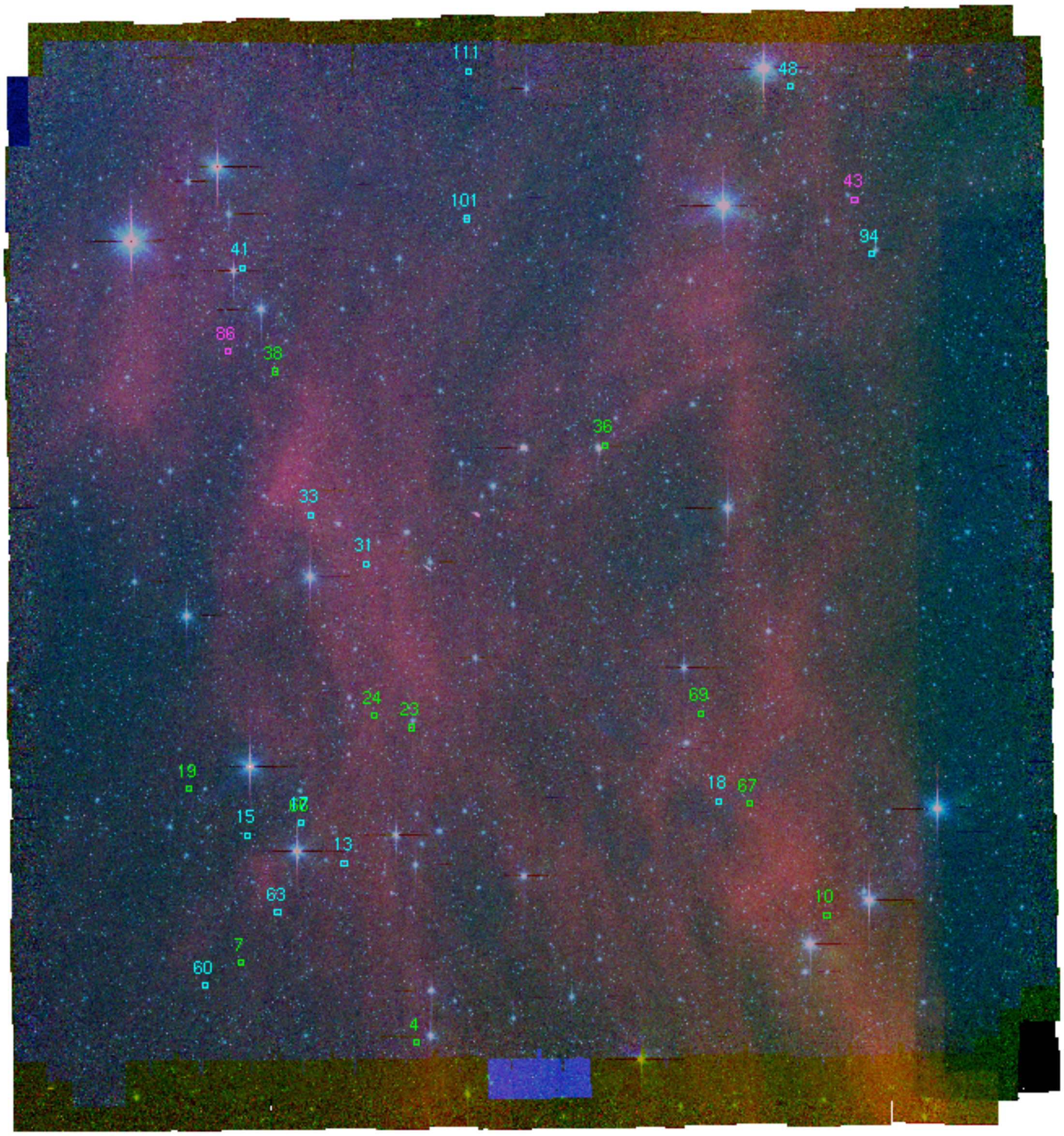

Figure 6-1. Positions of our best YSO candidates on the IRAC combined three-color image. Note that the majority of the best candidates are located near and within the cloud structure. Colors are based on spectral indices: Class 0/I (magenta), “Flat” (green), and Class II (light blue).

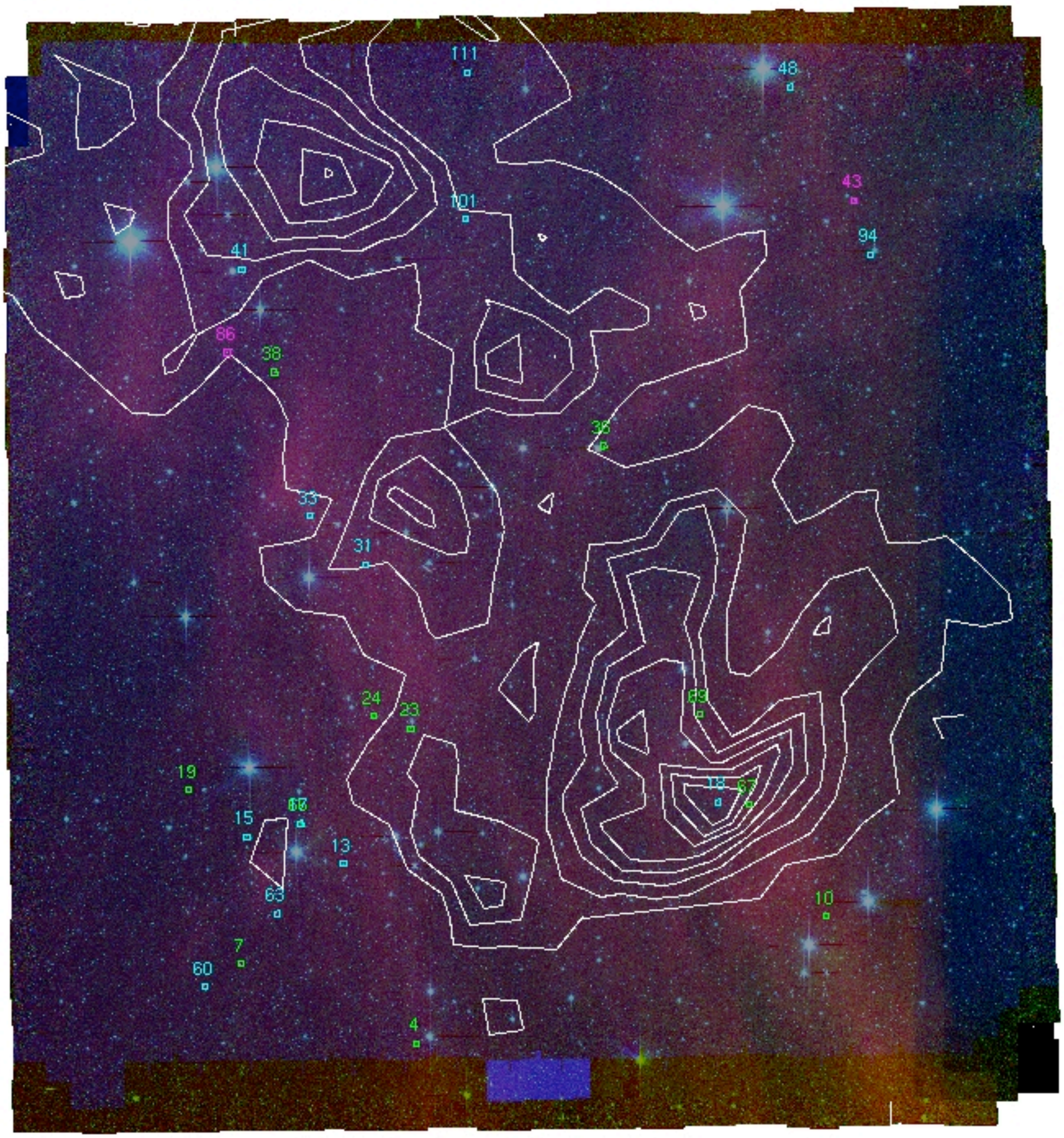

Figure 6-2. Best YSO candidates and CO(1-0) contours (see Figure 3-9) plotted on the IRAC three-color image.

6.3 Future Work

Many interesting candidate YSOs have been established by our search criteria using Spitzer images, but the confirmation of these sources as YSOs is difficult to perform with infrared data alone. While this data can be extremely useful, and vital in many cases, follow-up work must be considered to confirm a source's YSO status. Two methods that could be utilized to confirm or deny a candidate's YSO status involve spectroscopy. Signatures of a young star's spectra include strong Hα emission at 6563 Å and Lithium absorption at 6707 Å (Stahler & Palla 2004). Lithium absorption is a strong indicator because low-mass protostars to not have high enough temperatures to burn lithium, while main-sequence stars do. While Hα emission can certainly support evidence for YSO type objects, this emission also occurs in field dwarfs (Luhman and Steeghs 2004). Obtaining spectra of the most probable candidates and determining the presence or absence of both of these features could conclusively determine membership in MBM 12 young star association. A second possible future analysis of candidate members is a search for evidence of variability. Young stars can show brightness variation up to several magnitudes over time scales of days to about a week (Herbst et al. 2004). It has been shown by Herbst et al. (2004) that seven of the known YSOs within MBM 12 exhibit this trait, with some revisions of their rotational periods done by Broeg et al. (2006). If this feature could be established in any of the candidates we have listed, the likelihood of being a YSO would significantly increase. This type of observation can be carried out with a relatively small (meter class) telescope and a set of color filters, equipment that is available at the 0.9 m SARA telescope on Kitt Peak, AZ[12]. One further method that could be utilized to determine that a

[12] The University of Georgia has a portion of time available each year on the SARA telescope.

source is not a YSO returns us to the issue of background galaxy contamination. A survey of these sources with even higher resolution near-infrared or optical imaging could resolve sources more clearly, and possibly reveal if they are extragalactic in nature (i.e., by demonstrating that they are not point sources). We believe that any of these further investigations would assist significantly in our search for additional YSOs in MBM 12. In the meantime, our best YSO candidate catalog (Table 6-1) represents the ideal starting point for determining the complete star formation census of MBM 12.

REFERENCES

Allen, L.E., et al., *Infrared Array Camera (IRAC)) Colors of Young Stellar Objects*. Astrophysical Journal Supplement, 2004. **254**: pp. 363-366.

Andersson, B.G., R. Idzi, A. Uomoto, P.G. Wannier, B. Chen, and A.M. Jørgensen, *A Spectroscopic and Photometric Survey of Stars in the Field of L1457: A New Distance `Determination*. Astronomical Journal, 2002. **124**: pp. 2164-2177.

Böhm-Vitense, E., Introduction to Stellar Astrophysics. 1992, Cambridge: Cambridge University Press.

Briceño, C., et al., *X-Ray Surveys and the Post-T Tauri Problem.* Astronomical Journal, 1997. **113**: pp. 740-752

Broeg, C., et al., *Rotational Periods of T Tauri Stars in Taurus-Auriga, South of Taurus-Auriga, and in MBM 12*. Astronomy and Astrophysics, 2006. **450**: pp. 1135-1148

Caulet, A., R.A. Gruendl, and Y.H. Chu, *Young Stellar Objects in the Large Magellanic Cloud: N63 and N180 H II Regions*. Astrophysical Journal, 2008. **678**: pp. 200-218.

Chastain, R.J., R.L. Shelton, E.A. Raley, and L. Magnani, *A High-Latitude Molecular Structure In Pegasus-Pisces*. Astronomical Journal, 2006. **132**: pp. 1964-1976.

Dame, T.M., D. Hartmann, and P. Thaddeus, *The Milky Way in Molecular Clouds: A New Complete CO Survey*. Astrophysical Journal, 2001. **547**: pp. 792-813.

Dickman, R.L., *A Survey of Carbon Monoxide Emission in Dark Cloulds*. Astrophysical Journal, 1975. **202**: pp. 50-57.

Fazio, G.G., et al., *The Infrared Array Camera (IRAC) for the Spitzer Space Telescope*. Astrophysical Journal Supplement, 2004. **154**: pp. 10-17.

Fleming, T.A., I.M. Gioia, and T. Maccacaro, *The Relation Between X-Ray Emission and Rotation in Late-Type Stars from the Perspective of X-Ray Selection*. Astrophysical Journal. **340**: pp. 1011-1023.

Gir, B.Y., L. Blitz, and L. Magnani, *The Association of High-Latitude Molecular Clouds with H I Gas*. Astrophysical Journal. **434**: pp. 162-183.

Greene, T.P., B.A. Wilking, P. Andre, E.T. Young, and C.J. Lada, *Further Mid-Infrared Study of the Rho Ophiuchi Cloud Young Stellar Population: Luminosities and Masses of Pre-Main-Sequence Stars*. Astrophysical Journal, 1994. **434**: pp. 614-626.

Hartmann, D., L. Magnani, and P. Thaddeus, *A Survey of High-Latitude Molecular Gas in the Northern Galactic Hemisphere*. Astrophysical Journal, 1998. **492**: pp. 205-212

Hartmann, L., et al., *IRAC Observations of Taurus Pre-Main-Sequence Stars*. Astrophysical Journal, 2005. **629**: pp. 881-896

Harvey, P.M., et al., The *Spitzer c2d Survey of Large, Nearby, Interstellar Clouds. II. Serpens Observed with IRAC*. Astrophysical Journal, 2006. **644**: pp. 307-325.

Hearty, T.J., Star Formation at High Galactic Latitude. Thesis (PhD.) University of Georgia, 1997.

Hearty, T.J., L. Magnani, J.P. Caillault, R. Neauhäuser, J.H.M.M. Schmitt, and J. Stauffer, *A Search for Star Formation in the Translucent Clouds MBM 7 and MBM 55*. Astronomy and Astrophysics, 1999. **341**: pp. 163-173.

Hearty, T.J., et al., *ROSAT PSPC Observations of T Tauri Stars in MBM 12*. Astronomy and Astrophysics, 2000. **353**: pp. 1044-1054

Hearty, T.J., M. Fernández, J.M. Alcalá, E. Covino, and R. Neauhäuser, *The Distance to the Nearest Star-Forming Clouds: MBM 12 and MBM 20*. Astronomy and Astrophysics, 2000. **357**: pp. 681-685.

Herbig, and G.H., Bell, *Catalog of Emission Line Stars of the Orion Population: 3: 1988*. Lick Observatory Bulletin 1111, 1988.

Herbst, W., E.C. Williams, and W.P. Hawley, *A Photometric Study of Stars in the MBM 12 Association*. Astronomical Journal, 2004. **127**: pp. 1594-1601.

Hobbs L.M., L. Blitz, and L. Magnani, *A Molecular Cloud in the Local, Hot Interstellar Medium*. Astrophysical Journal, 1986. **306**: pp. L109-L113

Houck, J.R., et al., *The Infrared Spectrograph (IRS) on the Spitzer Space Telescope*. Astrophysical Journal Supplement, 2004. **154**: pp. 18-24.

Jørgensen, et al., *The Spitzer c2d Survey of Large, Nearby, Interstellar Clouds. III. Perseus Observed with IRAC*. Astrophysical Journal, 2006. **645**: 1246-1263.

Lada, C.J., *Star Formation – From OB Associations to Protostars*. Star Forming Regions; Proceeding of the Symposium, Tokyo, Japan, 1987.

Landsman, W.B., *The IDL Astronomy User's Library*. Astronomical Data Analysis Software and Systems II, A.S.P. Conference Series, 1993.

Liljestrom, T., *The High Latitude Cloud L1642 is Not Breaking Up*. Astronomy and Astrophysics, 1991. **244**: pp. 483-491.

Luhman, K.L., *On the MBM 12 Young Association*. Astrophysical Journal, 2001, 560: pp. 287-306.

Luhman, K.L., and D. Steeghs, *Spectroscopy of Candidate Members of the η Chamaeleontis and MBM 12 Young Associations*. Astrophysical Journal, 2004. **609**: pp. 917-924

Lynds, B.T., *Catalogue of Dark Nebulae*. Astrophysical Jounal Supplement, 1962. **7**: pp 1-62.

Magnani L., D. Hartmann, S.L. Holcomb, L.E. Smith, and P. Thaddues, *A Survey of High-Latitude Molecular Gas in the Southern Galactic Hemisphere*. Astrophysical Journal, 2000. **535**: pp. 167-175.

Magnani, L., L. Blitz, and L. Mundy*, Molecular Gas at High Galactic Latitudes*. Astrophysical Journal, 1985. **295**: pp. 402-421.

Magnani, L., D. Hartmann, and B.G. Speck, *A Catalog of Molecular Gas at High Galactic Latitudes*, Astrophysical Journal Supplement, 1996. **106**: pp. 447-461.

McGehee, P., *Star Formation and Molecular Clouds at High Galactic Latitude*. Handbook of Low Mass Star Forming Regions, A.S.P. Conference Series, 2008.

Ogura, K., et al., *Four Probable T Tauri Stars in MBM 12*. Publications of the Astronomical Society of Japan, 2003. **55**: pp. L49-L52.

Pound, M.W., R.W. Wilson, T.M. Bania, *Subparsec Clumping in the Nearby Molecular Cloud MBM 12*. Astrophysical Journal, 1990. **351**: pp.165-175

Reach, W.T., et al., *Protostars in the Elephant Trunk Nebula*. Astrophysical Journal Supplement, 2004. **154**: pp. 385-390.

Reach, W.T., et al., *Absolute Calibration of the Infrared Array Camera on the Spitzer Space Telescope*. Publications of the Astronomical Society of the Pacific, 2005. **117**: pp. 978-990.

Rho, J., W.T. Reach, B. Lefloch, and G.G. Fazio, *Spectacular Spitzer Images of the Trifid Nebula: Protostars in a Young, Massive-Star-Forming Region*. Astrophysical Journal, 2006. **643**: pp. 965-977.

Rieke, G.H., et al., *The Multiband Imaging Photometer for Spitzer (MIPS)*. Astrophysical Journal Supplement, 2004. **154**: pp. 25-29.

Rowan-Robinson, M., et al., *Spectral Energy Distributions and Luminosities of Galaxies and Active Galactic Nuclei in the Spitzer Wide-Area Infrared Extragalactic (SWIRE) Legacy Survey*. Astronomical Journal, 2005. **129**: pp. 1183-1197.

Sandell, G., B. Reipurth, and G. Gahm, *Low-mass Star Formation in the High Latitude Dark Cloud L1642*. Astronomy and Astrophysics, 1987. **181**: 283-288.

Sanders, D.B., and I.F. Mirabel, Luminous Infrared Galaxies. Annual Review of Astronomy and Astrophysics, 1996. 34: pp. 749-792.

Schlegel, D.J., D.P. Finkbeiner, and M. Davis, *Maps of Dust Infrared Emission For Use in Estimation of Reddening and Cosmic Microwave Background Radiation Foregrounds*. Astrophysical Journal, 1998. **500**: pp. 525-553.

Shu, F., F.C. Adams, and S. Lizano, *Star Formation in Molecular Clouds – Observation and Theory*. Annual Review of Astronomy and Astrophysics, 1987. **25**: pp. 23-81.

Skrutskie, R.M. et al., *The Two Micron All Sky Survey (2MASS)*. Astrophysical Journal, 2006. **131**: pp. 1163-1183.

Smith, M.D., *The Origin of Stars*. 2004, London: Imperial College Press. pp. 1-248.

Stahler, S.W., and F. Palla, The Formation of Stars. 2004, Weinheim: WILEY-VCH. pp. 1-822

Stephenson, C.B., *New H-alpha Emission Stars Found Above 10 Deg Galactic Latitude*. Astrophysical Journal, 1986. **300**: pp. 779-784.

Straizys, V., K. Cernis, A. Kazlauskas, and V. Laugalys, *Photometric Investigation of the MBM 12 Molecular Cloud Area in Aries. II. Cloud Distance*. Baltic Astronomy, 2002. **11**: pp. 231-247.

Strom, S.E., *Optical and Infrared Observations of Young Stellar Objects – an Informal Review*. Publications of the Astronomical Society of the Pacific, 1972. **84**: pp. 745-756

van Dishoeck, E.F. and J.H. Black, *The Photodissociation and Chemistry of Interstellar CO*. Astrophysical Journal, 1988. **334**: pp. 771-802.

Whitney, B.A., K. Wood, J.E. Bjorkman, and M. Cohen, *Two-Dimensional Radiative Transfer in Protostellar Evelopes. II. An Evolutionary Sequence*. Astrophysical Journal, 2003. **598**: pp. 1079-1099.

Zimmerman, T., H. Ungerechts, A Complete CO Map of the Nearest Molecular Cloud, L1457. Astronomy and Astrophysics, 1990. 238: pp. 337-346